The present work was submitted to DLR - Institute of Solar Research, Chair of Solar Technology

Bachelor thesis

Presented by Maurice Feulbach

Matriculation number: 392907

Experimental investigation of hydrogen reduction in PTC receivers by back-permeation into HELISOL® XLP silicone based HTF with accompanying venting of the HTF

Almería, February 2024

Name of 1st examiner: Univ.-Prof. Dr.-Ing. Robert Pitz-Paal

Name of 2nd examiners: Dr. Lukas Heller and Christoph Hilgert

Abstract

Hydrogen accumulation in Parabolic Trough Collector (PTC) receivers can significantly increase their heat losses and reduce PTC power plant efficiency and revenue. An experimental demonstration of hydrogen reduction in PTC receivers to restore their performance by hydrogen back-permeation into the heat transfer fluid (HTF) is set up at the KONTAS PTC test rig at the Plataforma Solar de Almería (PSA), Spain.

Within this thesis KONTAS is adapted for the experiment and an operation and data evaluation strategy is developed. The operation parameters are selected to simulate conditions of a PTC power plant changing its HTF from the state-of-the-art DPO/BP to the silicone based HTF HELISOL® XLP. An expansion vessel venting procedure is developed to reduce the hydrogen concentration in the HTF, which is required to enable hydrogen back-permeation from the receivers to the HTF. It is observed that the amount of condensate formed during venting significantly increases with higher venting temperatures. To balance expansion vessel cooldown time and condensate formation, the venting temperature is set at 150 °C. Analysis of HTF samples show that a 40 % reduction of hydrogen concentration in the HTF is achieved through the developed venting procedure. During operation the HCEs glass envelope temperatures are measured and graphically visualized so potential long term-changes of HCE heat losses can be detected. At the submission time of this thesis, the experiment just started and KONTAS had been in operation for 175 hours of the expected 3000 hours. So far, no HCE temperature reduction has been observed.

Table of Contents

Abstract I
Table of Contents II
1. Introduction 1
2. State of the art 3
2.1 Concentrating solar power 3
2.2 Parabolic trough power plants 4
2.3 Parabolic trough collectors 6
2.4 Heat transfer fluids for parabolic trough power plants 8
2.5 Hydrogen permeation into heat collecting elements 10
2.6 Hydrogen detection 14
2.7 Hydrogen reduction in the HTF 15
2.8 Hydrogen back-permeation from HCE to HTF 16
3. Experimental Setup 18
3.1 Purpose of experiment 18
3.2 KONTAS facility 18
3.3 Adaption of KONTAS for back-permeation test 19
3.3.1 Installation of hydrogen filled HCEs 19
3.3.2 Doting of HELISOL® XLP with DPO/BP 20
3.3.3 Sampling, recirculation and venting system 20
3.3.4 HCE Temperature Measurements 22
4. Development of operation and data evaluation strategies 23
4.1 Operation parameters 23
4.2 Venting and sampling strategy 24
4.2.1 Effect of venting temperature on formation of condensate 24
4.2.2 Venting procedure during operation 26
4.2.3 Venting control and frequency 28
4.3 Method to analyze HCE temperature data 30
5. Conclusion and Prospect 34
Nomenclature III
List of figures IV
List of tables V
List of references VI

1. Introduction

The energy sector is accountable for annual Green House Gas (GHG) emissions of 41.3 Gt CO_2 equivalents (International Energy Agency, 2023), which is around 70 % of the annual global net anthropogenic GHG emissions of 59 ± 6.6 Gt CO_2 equivalents (IPCC, 2022). A transition to a renewable based energy system is necessary to reach a sharp reduction of GHG emissions to limit the global warming to 1.5 °C. To this objective 196 parties committed in the Paris Agreement 2015, which was recently reaffirmed at the UN Climate Change Conference in Dubai, United Arab Emirates (COP 28) in 2023 (UNFCCC, 2023). Wind and photovoltaic (PV) are expected to provide the largest share of energy in a future decarbonized, renewable based energy system (Acatech/Leopoldina/Akademienunion, 2022) and in 2022 the construction of wind and solar PV made up 92 % of the renewable capacity increase (REN21, 2023). However, due to the inherent inconsistency of their primary energy source and the limited storage capacity of electricity, a high share of these variable renewable energy sources in the power generation system necessitates power system flexibility (IRENA, 2022b). Concentrating Solar Power (CSP) with thermal energy storage (TES) can offer flexibility on the power supply side by providing dispatchable, carbon neutral power and the ability to help balancing fluctuating renewables (Resch et al., 2022). Under the IRENA (2022b) 1.5 °C scenario the global CSP capacity will grow significantly from 6.1 GW_{el} in 2021 to 200 GW_{el} in 2030. Parabolic trough collector (PTC) power plants make up more than 75% of operating CSP plants (REN21, 2023).

To transfer the heat from the solar field to the power block and to the TES the eutectic mixture DPO/BP, consisting of diphenyl oxide (DPO) and biphenyl (BP) is the most commonly used heat transfer fluid (HTF) in state-of-the-art PTC power plants. But the steadily increasing degradation of DPO/BP causes the formation of low boiling compounds and gases, such as hydrogen, methane and carbon monoxide. Hydrogen is able to permeate into the vacuum between the glass envelope and the absorber tube of the heat collecting elements (HCEs) of the PTC power plants (Jung & Senholdt, 2020), which leads to an significant increase of thermal losses. This effect can lower the annual plant revenue by up to 20 % (Li et al., 2012). Mehos et al. (2020) stated that the receivers hydrogen accumulation is the main issue for parabolic trough technology.

New silicone based HTFs, such as the newly developed HELISOL® XLP from WACKER, have a higher upper operating temperature limit than DPO/BP and are expected to reduce the levelized cost of energy (LCOE) of new parabolic trough plants by up to 5 % (Jung et al., 2015). Furthermore, they show a higher chemical stability and a lower long-term hydrogen generation, which significantly reduces the hydrogen permeation into the HCEs. The reduced hydrogen formation compared to DPO/BP can improve the performance and lifetime of the HCEs and can reduce the intensity of hydrogen removal in existing power plants after replacing the DPO/BP with silicone based HTF (Jung & Senholdt, 2020; Jung et al., 2019).

The research project *High-performance parabolic trough collector and innovative silicone fluid for CSP power* (Si-CO) of the German Aerospace Center (DLR) further investigates the application of silicone based HTFs for existing and new PTC power plants. One part of the project is to investigate the mitigation of hydrogen in HCEs with hydrogen accumulation by back-permeation into the HTF. Hydrogen back-permeation means, that hydrogen is transferred back from hydrogen filled HCEs to the HTF, which can occur when the hydrogen partial pressure in the HTF is below the hydrogen partial pressure in the HCEs glass annuli. If the hydrogen partial pressure in the HCEs is reduced the heat losses can decrease and the HCEs performance could be restored to the original value. To show the possibility of back-permeation after an HTF change over from DPO/BP to HELISOL® XLP, a research experiment is set up at the KONTAS test facility at the Plataforma Solar de Almería (PSA) in Spain. At KONTAS, which consists of a PTC module with an attached pumping, heating and cooling unit mounted on a rotatable

platform HELISOL® XLP is circulated through hydrogen-filled HCEs. The HTF is partly recirculated through an expansion vessel to diffuse hydrogen and other gaseous degradation products into the expansion vessels nitrogen gas phase, which can be exchanged by venting and refilling fresh nitrogen.

The objective of this thesis is the preparation and adaption of KONTAS and the development of the operation and data evaluation strategies for the described experiment. The operation parameters will be selected to imitate conditions in a power plant changing its HTF from DPO/BP to HELISOL® XLP. Furthermore, an expansion vessel venting procedure will be developed to reduce the hydrogen concentration in the HTF during operation to enable back-permeation from the HCEs. The effectiveness and the frequency of the venting will be controlled with HTF samples, which are remote analyzed for their hydrogen concentration. Additionally, the HCE temperatures will be measured to detect long-term changes of HCE temperatures, indicating a reduction of hydrogen in the HCEs.

2. State of the art

2.1 Concentrating solar power

Solar thermal systems are used to capture and convert sunlight into usable thermal energy. By interposing optical devices such as mirrors or lenses the solar light can be concentrated and the size of the absorption area, where thermal losses occur, can be decreased. Thus, concentrating systems can achieve higher temperatures than non-concentrating ones. Different collector designs and shapes are used, depending on the application and the desired concentration factor, which is the ratio of the collector aperture area to the absorption area (John A. Duffie, 2013).

CSP plants use turbines or other heat engines to transform the absorbed heat into mechanical energy, which can be used by a generator to generate electricity. There are four main technologies available for concentrating solar power generation: Linear Fresnel reflectors (LFR), Parabolic Trough Collectors (PTC), Solar Tower (ST) systems and parabolic dish (PD) solar collectors (International Energy Agency, 2010). However, only LFR, PTC and ST systems are currently used in operational power plants (National Renewable Energy Laboratory, 2022). LFR and PTC are line focusing technologies with linear rows of mirrors and absorber tubes, whereas solar tower and parabolic dish systems are point focusing with a central receiver. Figure 1 shows the working principle of these technologies.

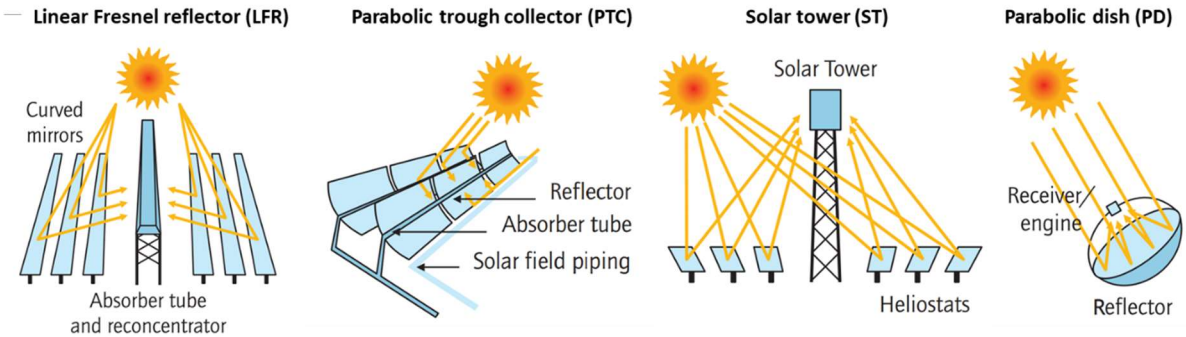

Figure 1: Types of CSP power plants. Credit: (International Energy Agency, 2010)

The main advantage of CSP, which makes it stand out from volatile renewable energy technologies such as wind power and PV, is that the thermal energy can be stored with TES systems in a large scale to enable dispatchability and electricity supply on demand (Alami et al., 2023). CSP-TES systems provide economic benefits over PV systems with battery electric storage for storage periods of more than 2 h to 3 h at current costs and for periods greater than 4 h to 10 h with estimated cost for the year 2040 (Schöniger et al., 2021).

As CSP systems can only use direct radiation especially areas with high direct normal irradiation (DNI) are suited for CSP (Alami et al., 2023). In 2022 a global CSP capacity of 6.3 GW_{el} was in operation, from which 2.3 GW_{el} are in Spain and 1.3 GW_{el} in the US. The largest capacity growth takes place in China, with a scheduled increase of 1.4 GW_{el} in 2023 (REN21, 2023). Under the IRENA 1.5 °C scenario the global CSP capacity will grow 30 fold from 6.1 GW_{el} in 2021 to 200 GW_{el} in 2030 (IRENA, 2022b). However, the future of CSP depends heavily on the national policies in the sunbelt countries, especially in the major markets China and Spain (Lilliestam et al., 2020). Also, further cost reductions are crucial for CSP. The LCOE of CSP projects decreased by 68 % from an average price of 0.358 USD/kWh in 2010 to 0.114 USD/kWh in 2021 (IRENA, 2022a).

Globally PTC technology is the most mature and most widely used CSP technology as it makes up more than 75 % of CSP plants (REN21, 2023) and produces approximately 70 % of CSP generated electricity (Awan et al., 2020)

2.2 Parabolic trough power plants

A PTC power plant consists of a solar field, a power block (PB) and a TES system (Alami et al., 2023). The schematic structure is shown in Figure 2.

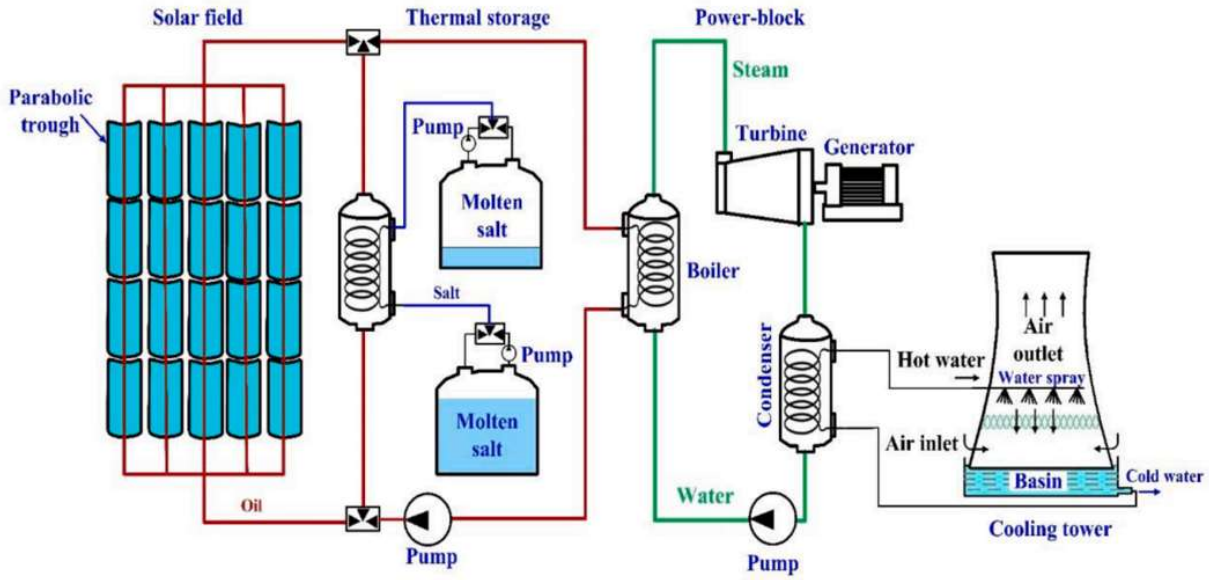

Figure 2: Schematic structure of a PTC power plant. Graphic from (Alami, Olabi et al. 2023)

The typically rectangular shaped solar field is made up of numerous 250m to 300 m long parallel rows of north-south oriented PTC Collectors. Each two adjacent rows of collectors are connected in a loop with a resulting length of 500m to 600 m which start and end at the east-west orientated supply lines respectively return lines. (Mehos et al., 2020). In most PTC power plants Diphenyloxid /Biphenyl (DPO/BP) is used as the HTF. Commonly, it enters the loops from the cold supply line at a temperature of 293 °C and leaves the collectors at the return line with a temperature of 393 °C (Awan et al., 2020).

The HTF transports the heat from the solar field to the heat exchanger of the TES system or of the PB. The TES system is used to store surplus thermal energy from the solar field, which can be transferred to the PB at a later time. Thus, a TES can provide dispatchability and increase the PB capacity factor by extending operation to non-sun hours (Alami et al., 2023).

The most mature technology for TES systems of PTC power plants is the dual-tank indirect molten salt (MS) TES (Awan et al., 2020). This system consists of one or several hot and cold tanks and an HTF-MS heat exchanger. To charge the TES, hot HTF flows through one side of the heat exchanger, while cold MS flows from the cold tank through the other side of the heat exchanger to the hot tank. Thus, the temperature of the HTF decreases while the temperature of the molten salt increases. For discharging the TES, the flow directions are reversed, so the MS flows from the hot to the cold tank and transfers heat to the HTF (Alami et al., 2023; Awan et al., 2020).

To generate electricity, the heat from the solar field or the TES is transported by the HTF to the heat exchanger of the power block. Most PTC power plants use a Rankine cycle to covert the thermal energy into mechanical energy to power an electric generator. Around 85 % of PTC generated electricity is

produced with steam Rankine cycles which use water as a working fluid (Awan et al., 2020). Figure 2 shows the typical rectangular layout of a PTC plant and its main components.

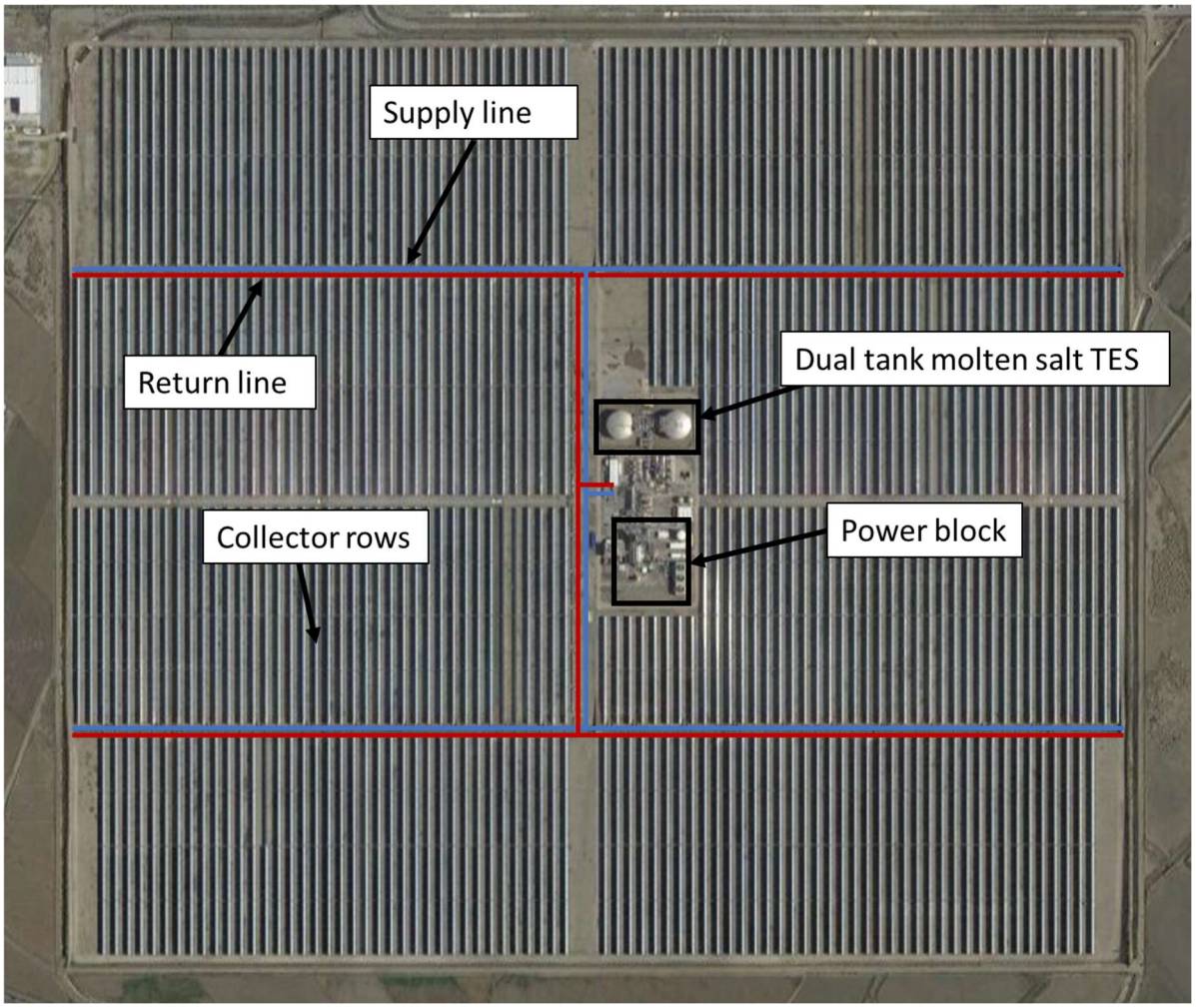

Figure 3: PTC plant Andasol 2 with marked supply line (blue) and return line (red). Photo from Google maps, based on (Mehos et al., 2020)

The typical PTC power plant configuration is a power block with 50 – 200 MW electrical power and a 6 to 10 h dual-tank MS TES. The average annual solar-to-electricity efficiency of PTC power plants is around 11 % to 16 % (Schöniger et al., 2021).

The overall power plant efficiency is mainly limited by the HTF, as its thermal stability determines the plant's maximum operation temperature and thus, the reachable efficiency of the Rankine process. Appropriate HTFs with high operation temperature increase the power block efficiency and reduce sizing and cost of heat exchangers, TES system and receivers (Awan et al., 2020). At the same time higher operating temperatures lead to higher heat losses. Accordingly, there is an design and location specific optimum operating temperature (Navas, Ollero, & Rubio, 2017).

2.3 Parabolic trough collectors

Parabolic trough collectors are line focusing collector systems with typical concentration factors between 50 and 90. The main components are parabolic reflectors, receiver tubes, a supporting structure, a tracking system and a heat transfer fluid (Desai & Bandyopadhyay, 2016).

The parabolic shaped reflectors made of silvered glass, polished aluminum or silvered polymers focus the DNI on a so-called heat collecting element (HCE), located in the focal line of the parabolic reflector. The HCE converts the concentrated solar light into heat and transfers it to the HTF, which flows through the HCEs. To hold the reflector and the HCEs in their position and shape and to provide the necessary stability to withstand wind loads and torsion, a supporting structure mostly made from steel or aluminum is used. As only direct beam radiation can be concentrated by the parabolic collector a solar tracking system is needed to increase the energy gain (Tagle-Salazar, Nigam, & Rivera-Solorio, 2020). Figure 4 shows the working principle of a PTC.

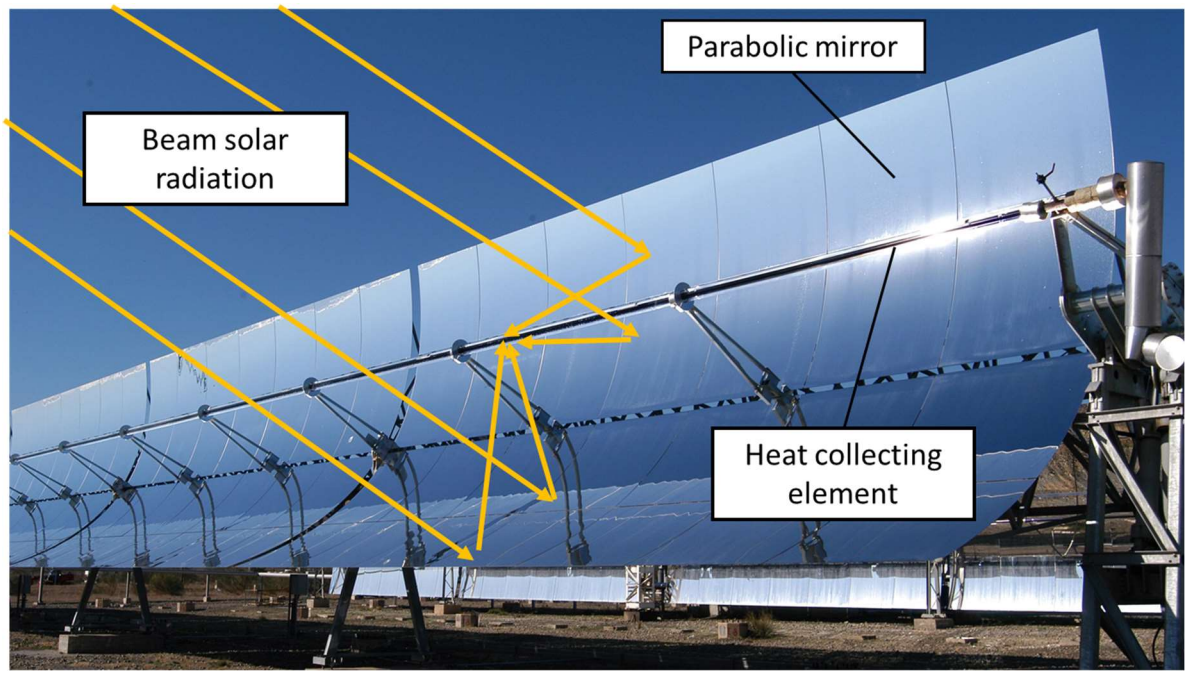

Figure 4: Working Principle of PTC. Credit for photo: DLR (edited)

The HCEs main functions are maximizing the absorption of radiation, enabling the heat transfer to the HTF and minimizing thermal losses caused by convection and radiation. To increase the thermal efficiency of the HCEs selective coatings on the absorber tube are used to increase the absorption of radiation in the solar spectral range while decreasing the emissivity at operating temperature to reduce thermal radiation losses. Thermal losses by convection are reduced by covering the absorber tube with a glass envelope, mostly made from Borosilicate glass with antireflective coating. As shown in Figure 5 the annular gap between the glass envelope and the absorber tube is evacuated to further reduce conduction and convection losses (Lang et al., 2017).

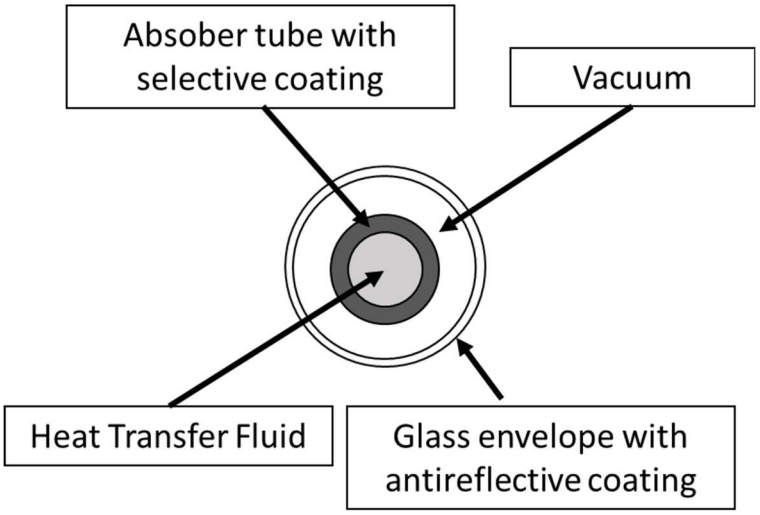

Figure 5: Cross-section of Heat Collecting Element

Airtight bellows at the connection between glass envelope and absorber tube allow thermal expansion differences while still holding the vacuum. To maintain the vacuum a chemical active substrate, called getter, is placed inside the vacuum to absorb intruding gases such as hydrogen, which can be formed as a degradation product in the HTF and permeate through the absorber tube into the vacuum (Tagle-Salazar, Nigam, & Rivera-Solorio, 2020). The hydrogen formation and permeation are further explained in chapter 2.5. A commonly used getter material for PTC applications is Zirconium (Lang et al., 2017). As a saturation of the getter and a loss of the vacuum increase the thermal losses of HCEs significantly the condition of the vacuum is mainly responsible for the HCEs lifetime. Hydrogen barrier coatings on the absorber tube can slow down the hydrogen permeation rate and thus can enlarge the HCEs lifetime (Li et al., 2012). Figure 6 shows the structure of an HCE.

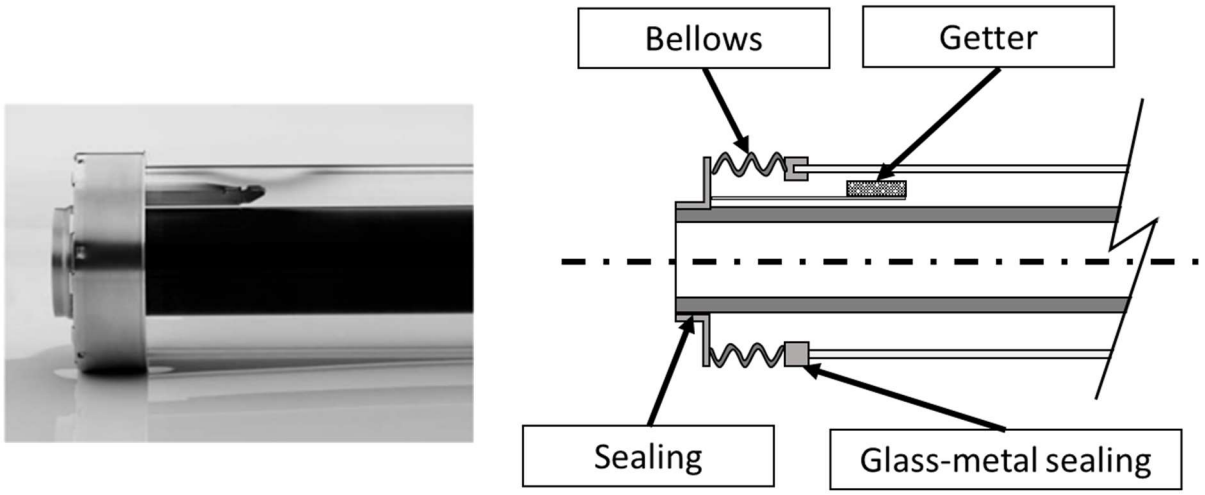

Figure 6: structure of Heat Collecting Element (photo on the left from SCHOTT Solar CSP GmbH)

The overall optical efficiency of PTCs, considering reflectivity of the mirrors, transmission through the glass envelope and absorption of the receiver tube, is around 75 % (Awan et al., 2020).

2.4 Heat transfer fluids for parabolic trough power plants

To enable an efficient heat transfer from the solar field to the power block and to the TES, there are numerous requirements for the HTF. An HTF ideally has a high thermal capacity and conductivity, a low thermal expansion and viscosity, combined with a low toxicity and a high thermal and chemical stability. Additionally, a low melting point, a high boiling point and a low vapor pressure are desired to extend the operating temperature range and avoid unwanted phase changes (Krishna et al., 2020; Tagle-Salazar, Nigam, & Rivera-Solorio, 2020).

Liquid water can be used as a low environmental risk HTF especially in low-temperature applications below around 250 °C, for higher temperatures the increasing vapor pressure of water causes the need for components with a higher pressure rating, which are increasingly costlier. Steam can be used in PTC fields up to 500 °C, but the two-phase flow of water and steam, as used for direct steam generation requires a more complex flow control and can cause receiver tube dry out and high temperature gradients, which can damage receiver tubes and the selective coating (Krishna et al., 2020; Tagle-Salazar, Nigam, & Rivera-Solorio, 2020). Also, the storage ability is limited by the low density of steam and the expensive high pressure stage required for the storage tanks of high temperature liquid water (Alami et al., 2023; Jung et al., 2015).

Pressurized gasses, such as hydrogen, carbon dioxide, helium and air are, due to their wide operating temperature range of up to 900 °C, considered for application as an HTF. The drawbacks of pressurized gases are a low energy density, a low thermal conductivity and a large power consumption for pumping. There are also difficulties regarding poor heat transfer from the receiver to the gas, suitable high temperature TES and the complex solar field control (Awan et al., 2020; Tagle-Salazar, Nigam, & Rivera-Solorio, 2020). Another investigated class of HTFs is the suspension of Nanoparticles, which are solid nanometer-sized particles, commonly made form metals or metal oxides such as CuO, Ag, SiO_2. The so called nanofluids based on water or thermal oil could improve the convective heat transfer coefficient and the thermal efficiency, but further research is necessary regarding different nanoparticles and their thermal performance and stability (Moosavian et al., 2023; Tagle-Salazar, Nigam, & Rivera-Solorio, 2020).

Molten salts can be applied as a storage medium as well as an HTF. As molten salts have a high thermal stability, a high specific heat capacity, a high density and a low vapor pressure even at temperatures up to 550 °C (Solar Salt), they have been used as HTF in solar tower applications since 1996. Compared to synthetic thermal oils they are cost-effective and have a lower environmental impact (Awan et al., 2020). Molten salts as an HTF can eliminate the heat exchanger between the solar field and the TES and increase the operating temperature of the steam cycle to up to 540 °C, which increases the power block efficiency accordingly (Desai & Bandyopadhyay, 2016). Due to the increased power cycle efficiency and the direct thermal energy storage an estimated LCEO reduction of 20 % could be achieved by switching from the state-of-the-art thermal oil DPO/BP to molten salt as an HTF (Pan et al., 2018). However, the application of molten salts as an HTF for PTC power plants causes numerous challenges. The freezing point of the most commonly used Solar Salt, a binary mixture of 60 wt.% $NaNO_3$ and 40 wt.% KNO_3 is 220 °C and around 120 °C for specially developed low freezing temperature ternary salts such as Hitec® XL (Pan et al., 2018). Thus, additional insulation and a costly anti-freezing system for the solar field of PTC plants is required (Desai & Bandyopadhyay, 2016). Also corrosion of steel components such as pipes, valves, tanks and welding joints is an issue of molten salts (Awan et al., 2020). Research and testing are ongoing regarding different salt compositions and freeze protections methods, such as temporary water dilution to keep the salt liquid during filling or in emergency situations (Krüger et al., 2024; Naresh et al., 2022).

Thermal oils are the most commonly used HTF in PTC power plants and can be divided into mineral oils made in refining processes from crude oil, synthetic oils which are produced by chemical synthesis, and other oils of different kind for example non-hydrocarbon-based oils, such as silicon based oils (Giaconia et al., 2021).

Mineral oils are relatively inexpensive, as they are often a by-product from refining processes. They have a relatively low viscosity and density and provide stability against thermal degradation and oxidation at an operating temperature range of -10 °C to 300 °C (Tagle-Salazar, Nigam, & Rivera-Solorio, 2020).

Synthetic oils can be used in a wider temperature range between -90 °C and 400 °C. Thus, no freezing protection is required and higher operation temperatures and higher power plant efficiencies than with mineral oils can be achieved (Tagle-Salazar, Nigam, & Rivera-Solorio, 2020). The eutectic mixture of 72 % to 75 % diphenyl oxide (DPO) and 25 % to 28 % biphenyl (BP), which is sold under the tradenames Therminol® VP-1, Dowtherm™ A and Diphyl®, is used in most commercial parabolic trough plants (Jung et al., 2015; Schaffer et al., 2016). The disadvantages of DPO/BP are environmental and occupational risks manly due to the formation of Benzene and Benzol. Furthermore, the thermal degradation at operating conditions leads to the formation of degradation products such as hydrogen, which can, as further described in chapter 2.5, permeate into the vacuum insulation of the HCEs and increase the thermal losses drastically. As the ageing process of DPO/BP is highly temperature dependent, the upper operating temperature is normally set to 393 °C (Jung & Senholdt, 2020; Jung & Spenke, 2022).

To further increase the HTFs operating temperature and to lower the degradation- and hydrogen formation rate silicone based HTFs were developed. Silicone based HTFs such as HELISOL® 5A, as well as its improved versions with lower vapor pressure HELISOL® 10A, HELISOL® XA and HELISOL® XLP from WACKER, which are linear, clear, odorless and non-reactive polydimethylsiloxanes have an increased thermal stability and allow a broad temperature range of – 40 °C to 425 °C (Wacker Chemie AG, 2020). The increased maximum operating temperature leads to a higher possible efficiency of the Rankine cycle and to a smaller storage system at the same capacity compared to DPO/BP. A techno-economic comparison by Jung et al. (2015) shows a 5% reduction potential of the LCOE when switching to HELISOL® .

As shown in Figure 7, HELISOL® 5A at 400 °C as well as at 425 °C has a considerably slower formation of hydrogen compared to the state of the art used DPO/BP at 400 °C. (Jung et al., 2015; Wacker Chemie AG, 2020). Furthermore, according to Figure 7 and as further described in Chapter 2.5 the hydrogen formation rate of DPO/BP significantly increases with time, whereas the hydrogen formation rate of HELISOL® 5A decreases.

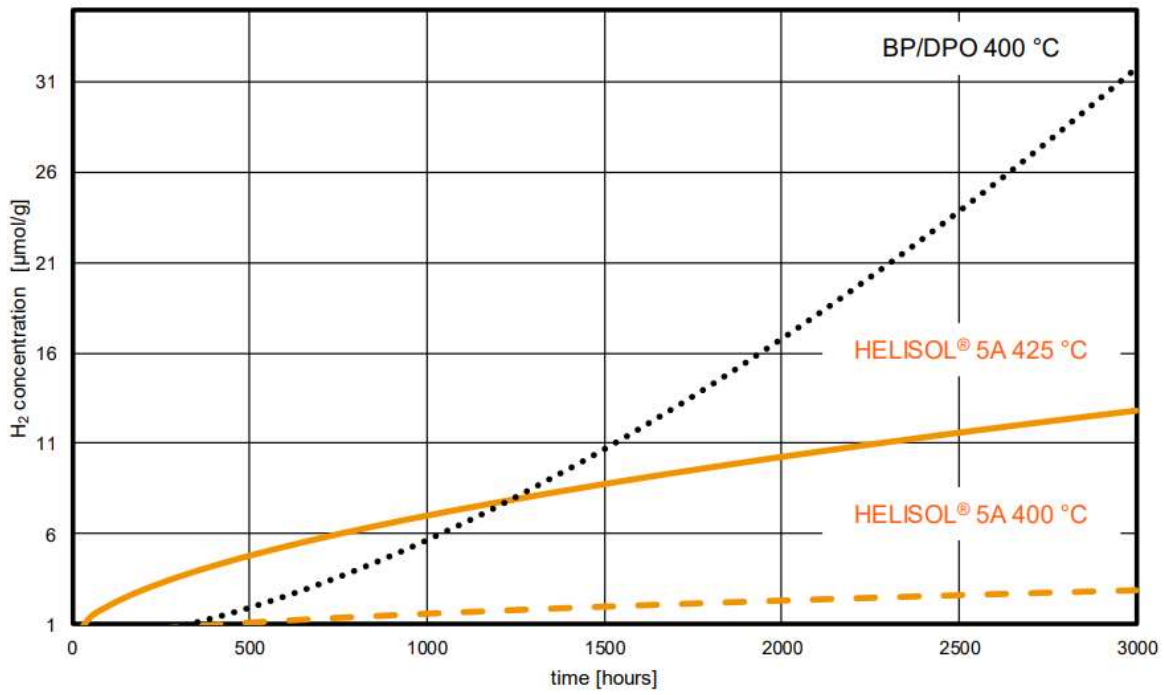

Figure 7: Hydrogen formation of HELISOL® 5A and DPO/BP (Wacker Chemie AG, 2020)

The reduced hydrogen formation could increase the receiver lifetime and reduce the efforts of hydrogen removal. There is also no fouling of HELISOL® grades at operation temperature and unused silicon based HTF is classification-free in the Globally Harmonized System of Classification and Labeling of Chemicals (GHS). But when used above 220 °C low-volatile components with different toxicological and flammability ratings as the unused fluid format (Wacker Chemie AG, 2020). As research projects investigating HELISOL® HTFs started in 2012 (Schaffer, 2020), HELISOL® HTFs are relatively new and there is yet no commercial application in a power plant (NREL, 2024).

Overall thermal oil, particularly DPO/BP is the most commonly used HTF in state-of-the-art PTC power plants. Switching from DPO/BP to silicone based HTF could be achieved without major modifications in solar field design and with already available components (Jung et al., 2015) and offers a LCOE reduction potential of 5 %. Also, the hydrogen formation and permeation to the vacuum insulation of the HCEs could be reduced, which would increase the lifetime and efficiency of the HCEs (Jung et al., 2015). Due to the large LCEO reduction potential of 20 % (Pan et al., 2018) a change of PTC plant design to molten salt as an HTF is expected in the future (Dersch et al., 2020).

2.5 Hydrogen permeation into heat collecting elements

During PTC power plant operation at the typical temperature range of 293 °C to 393 °C slow thermal degradation of DPO/BP appears and gases such hydrogen, carbon monoxide and methane as well as several low and high boilers are formed. Molecular hydrogen is formed by radical chain reactions in DPO/BP, with a reaction rate exponentially increasing with temperature. The reaction rate of these radical reactions increases with the accumulation of phenol, one of the low boiling degradation products of DPO/BP. Thus, the hydrogen formation rate, if the phenol in not removed, steadily increases with time and further degradation of DPO/BP (Jung & Senholdt, 2020). Formation rates up to eight times as high as in unused HTF have been measured in samples taken from parabolic trough plants (Jung & Spenke, 2022).

At first, the hydrogen formed in the degradation process is entirely dissolved in the DPO/BP. As soon as the DPO/BP is locally saturated the additional formed hydrogen occurs in form of different sized bubbles, which flow with the HTF. When being at the inner surface of the absorber tube, hydrogen can permeate into the vacuum annulus. Figure 8 shows the schematic path of the hydrogen from the formation in the HTF to the vacuum annulus. The permeation consists of several steps of adsorption, dissociation, dissolution, diffusion, recombination and desorption. As the diffusion is much slower than the surface processes, it is the rate-controlling process of the permeation (Li et al., 2012). There are two diffusion mechanisms for the hydrogen. In the Interstitial mechanism H_2 breaks down into two H^+ ions, which are small enough to pass through the spaces in the lattice structure of the metal tube. The second mechanism is the substitutional mechanism, also called vacancy mechanism, according to which the hydrogen ions can diffuse through voids or vacancies in the latticework (Yokogawa Electric Corporation, 2022).

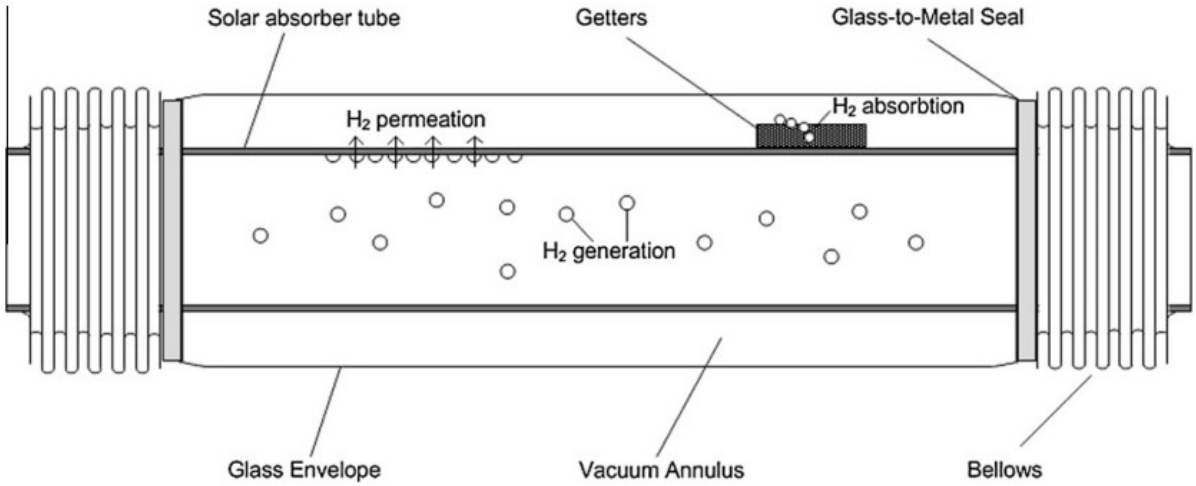

Figure 8: Hydrogen formation and permeation in HCEs. Graphic from (Li et al., 2012)

According to the permeation model for parabolic trough receiver tubes developed by Li et al. (2012), the permeation rate depends on the hydrogen permeation area, the absorber tube wall thickness, the hydrogen pressure in the vacuum annulus and the hydrogen concentration in the HTF as well as on the hydrogen permeability of the absorber tube including potential permeation barriers. The permeability Φ can be described using the Arrhenius relation, of the form $\Phi = \Phi_0 \exp(-E_p/\mathrm{RT})$, where Φ_0 is the permeability constant, E_p the hydrogen permeation activation energy, R the gas constant and T the temperature. As seen in this equation the permeability is a thermally activated process and increases exponentially with the temperature. Therefore, hydrogen generation and permeation processes are the highest at the hot end of the loops and can be neglected for low HTF temperatures at night (Li et al., 2012).

To absorb the hydrogen, which permeates through the steel absorber tube into the HCEs vacuum annulus, hydrogen getters have been installed in the vacuum annulus of HCEs, since the early days of PTC technology (Jung et al., 2019; Moens & Blake, 2010). To maintain the vacuum and to avoid the formation of a heat-conducting atmosphere inside the vacuum annulus for a HCE lifetime of 25 years, receiver suppliers defined a maximum hydrogen partial pressure of 30 Pa or 0.3 mbar in the vapor space above the HTF (Glatzmaier, 2020; Lang et al., 2017), which is equal to around 8 µmol H_2/kg of HTF (Jung & Spenke, 2022) or 1 ppb of dissolved hydrogen in DPO/BP at 40 °C (Lang et al., 2017).

However, it was observed in numerous PTC power plants that the hydrogen pressures inside the vacuum annuli can exceed the gas-absorbing capacity of the getters significantly (Moens & Blake,

2010). As stated by Lang et al. (2017) the hydrogen concentration under typical operating conditions already increases 0.7 ppb of the maximum tolerated 1 ppb each time the HTF flows through the solar field. Jung, Senholdt et al analyzed the hydrogen concentration in HTF samples from thirteen commercial PTC plants and observed that in 90 % of the samples the hydrogen concentration surpasses the HCE manufacturers limits. Under regular operating conditions, hydrogen concentrations were measured to exceed these limits more than hundredfold (Jung et al., 2019).

If the hydrogen concentration surpasses the limits of the receiver manufacturer, the hydrogen permeation exceeds the gas-absorbing capacity of the hydrogen getters, which leads eventually to a saturation of the getters and thus to an increase of hydrogen pressure inside the vacuum insulation (Moens & Blake, 2010).

The growing hydrogen pressure, and thus a growing number of molecules inside the vacuum annulus decreases the molecular mean free path length λ between the molecules. This decreases the dimensionless Knudsen number Kn defined as $Kn = {}^{\lambda}/_{L}$, in which L is the characteristic physical length of the space. The magnitude of the Knudsen number has a strong impact on the thermal conductivity, which is divided into four conduction ranges (see Figure 9). For $Kn > 10$ which is equal to a hydrogen pressure smaller than 0.1 Pa, the heat conduction is in the free molecular range. Due to the small number of molecules in the annular space the heat conduction in this region is very low. If the hydrogen pressure in the annulus is between 0.1 and 10 Pa the Knudsen number is between 0.1 and 10, which is called the transition region, because the conduction starts to increase significantly. For a further increase of hydrogen pressure to between 10 Pa and 100 Pa, the Knudsen number is in the temperature jump region between 0.01 and 0.1. There, the conductive heat losses grow almost linearly with increasing hydrogen pressure. Above 100 Pa of hydrogen pressure, which equals a Knudsen number below 0.01, the increase of heat conduction flattens and reaches a maximum in the continuum region (Lei, Ren, & Wang, 2020). Figure 9 shows the simulation results for the conductive heat losses of a heat transfer model developed for evacuated parabolic trough receivers by Lei, Ren and Wang. The HTF temperature in this case was set to a constant value of 350 °C.

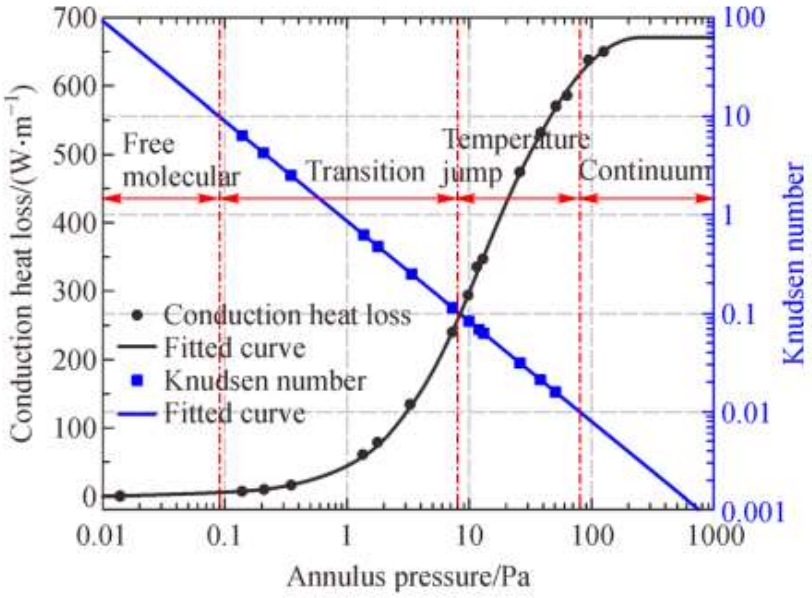

Figure 9: Conduction heat loss and Knudsen number as a function of the annulus pressure for an HTF temperature of 350 °C (Lei, Ren, & Wang, 2020)

The model shows that the conductive heat losses grow significantly from almost 0 to 670 W/m with an increasing hydrogen pressure in the vacuum annulus (See Figure 9), while the radiative losses, which are dominant for hydrogen pressures below 1 Pa, slightly decrease from about 145 to 125 W/m. The reduction of radiative losses is caused by the reduced radiative heat transfer between the absorber tube and the glass envelope due to the increasing temperature of the glass envelope, which rises significantly from around 340 K at 0.1 Pa hydrogen pressure to 428 K at above 1000 Pa (Lei, Ren, & Wang, 2020). Overall the increase of the conductive heat loss is much larger, than the reduction of radiative heat losses, so the total heat loss, as seen in Figure 10, increases significantly from 150 W/m to 800 W/m.

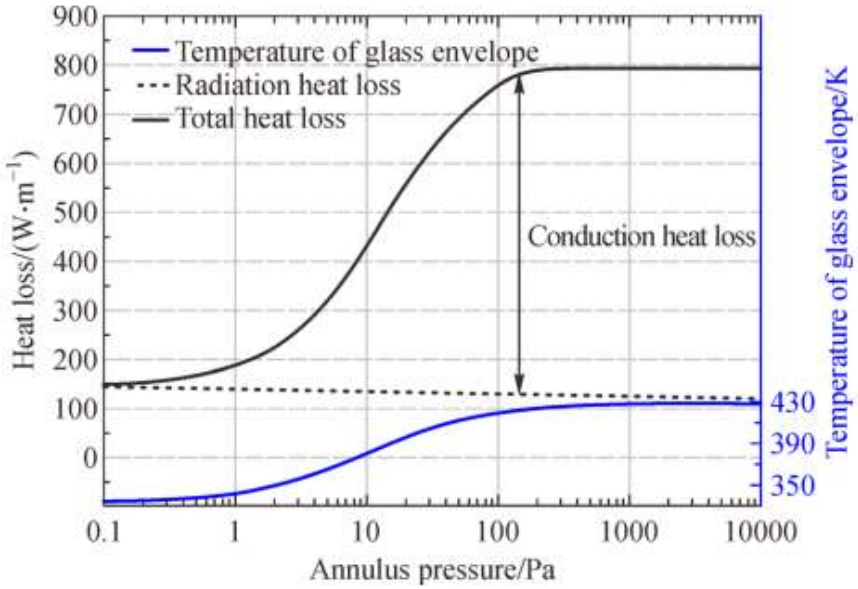

Figure 10: total heat loss and glass envelope temperature as a function of the hydrogen annulus pressure (Lei, Ren, & Wang, 2020)

Laboratory measurements of PTR70 parabolic trough receivers from Schott at 390 °C proof these simulation results, as the total heat loss increases four-fold from 220 W/m with intact vacuum to around 880 W/m at 133 Pa hydrogen pressure inside the receiver annulus (Burkholder & Kutscher, 2009; Lang et al., 2017). Glatzmaier, Cable and Newmarker (2017) also measured and compared heat losses of a receiver used in a power plant with an unused one and found similar significant increased thermal losses for used receivers.

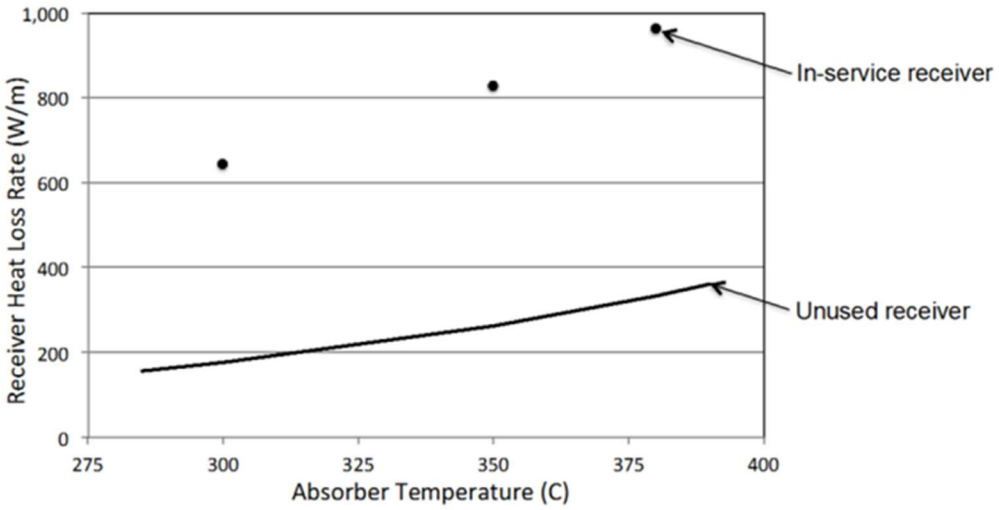

Figure 11: Receiver heat losses of unused and an in-service receiver at different temperatures (Glatzmaier, Cable, & Newmarker, 2017)

The increased heat losses of the HCEs lower the power plant efficiency and can reduce the plant revenue by up to 20 % (Li et al., 2012). Mehos, Price et al. stated that the receivers hydrogen accumulation is the main technical issue for parabolic trough technology (Mehos et al., 2020).

2.6 Hydrogen detection

To approach the issue of hydrogen accumulation in the receiver's vacuum annulus methods for hydrogen detection in the vacuum annulus, in the HTF and in the headspace gas of the expansion tank.

Vacuum indicators, made from barium and placed inside the HCEs annular gap can provide a very rough estimation on the vacuum condition by turning white when exposed to oxygen (Forristall, 2003). A loss of vacuum by hydrogen accumulation significantly increases the thermal conductivity and thus, increases the surface temperature of the glass envelope. By measuring this surface temperature with infrared cameras, hot receivers with high heat losses can be detected, but it is difficult to identify the type of infiltrated gas or its partial pressure (Yao et al., 2019). Another method to measure the glass surface temperature as well as the receiver tube temperature is the use of semi-cylindrical measurement headers with integrated sensors for the electromagnetic radiation emitted from the inner receiver tube and the outer glass tube. When laid on a receiver tube the semi-cylindrical header blocks radiation from the environment, so the sensors only measure the electromagnetic emissions from the receiver tube with a wavelength of below 3,5 µm and from the glass envelope with a wavelength above 4 µm (Espinosa-Rueda et al., 2016). The residual gas inside the glass envelope can be analyzed by a system consisting of a receiver tube opening device, a high vacuum system and a quadrupole mass spectrometer. But this method is destructive and can only be applied indoors (Yao et al., 2019).A non-destructive method to get further information about the gas composition inside the vacuum annulus is the application of a gas ionization and spectrometric analysis system. A high frequency power source generates a plasma inside the annulus by energizing the gas atoms to release free electrons and ions. When returning to the equilibrium state, the plasma emits light. By analyzing the wavelengths with a spectrometer, the atoms composing the plasma can be identifies by their emitted characteristic wavelength (Espinosa-Rueda et al., 2016; Yao et al., 2019). When measuring the voltage between the electrodes used for ionization the pressure inside the annulus can be determined with a relationship between voltage and pressure (Yao et al., 2019).

The hydrogen concentration in the HTF itself can be measured by extracting hot and pressurized HTF samples during the power plants operation. With this method the fluid and gas composition of the HTF is not changed during sampling. In offline-analyses using pressure measurement and gas chromatography the hydrogen concentration can be ascertained (Jung et al., 2019).

Another approach, developed by Glatzmaier (2018) is to measure the hydrogen pressure in the HTFs headspace of the expansion tank. In the patented method a palladium/silver (Pd/Ag) alloy membrane separates an initially evacuated permeate volume with a pressure gauge from the headspace gas flow. As the membrane is only permeable for hydrogen the same pressure as the hydrogen partial pressure in the head gas is established in the permeate volume. Thus, the hydrogen partial pressure in the headspace gas can be determined by measuring the pressure in the permeate volume.

2.7 Hydrogen reduction in the HTF

To reduce the hydrogen in the HTF different methods can be applied. As under ambient conditions typically more than 90 % of the hydrogen is located in the gas phase above the liquid, hydrogen can be removed from the HTF in PTC plants by decompressing after nightly cooldown and releasing the dissolved gases directly through the ullage system. Before heating up again fresh nitrogen needs to be fed in to replace the released gas and restore the pressure (Jung et al., 2019).

Another method is the hydrogen removal from the expansion vessel during the operation via flushing with nitrogen (Kuckelkorn et al., 2016). Contrary to the decompression the pressure inside the expansion vessel can be maintained during the flushing. Fresh nitrogen is fed into the expansion vessel and dilutes the prevalent vapor phase in the head space. Due to this dilution the partial pressure of the low boiling components including hydrogen in the vapor phase is reduced. As the Henry´s law states, there is a driving force transferring low boiling components and hydrogen from the liquid to the gas phase to increase its partial pressure to reach an equilibrium again. By this equilibration the hydrogen concentration in the HTF can be reduced by more than 80 % (Jung & Spenke, 2022). Thus, when leaving the expansion vessel, the nitrogen flow takes along the dissolved boiling components and hydrogen. Gases, low and high boilers are separated from the nitrogen flow in the ullage system and remaining HTF is returned to the cycle (Lang et al., 2017). Figure 12 illustrates the hydrogen removal from the HTF through nitrogen venting.

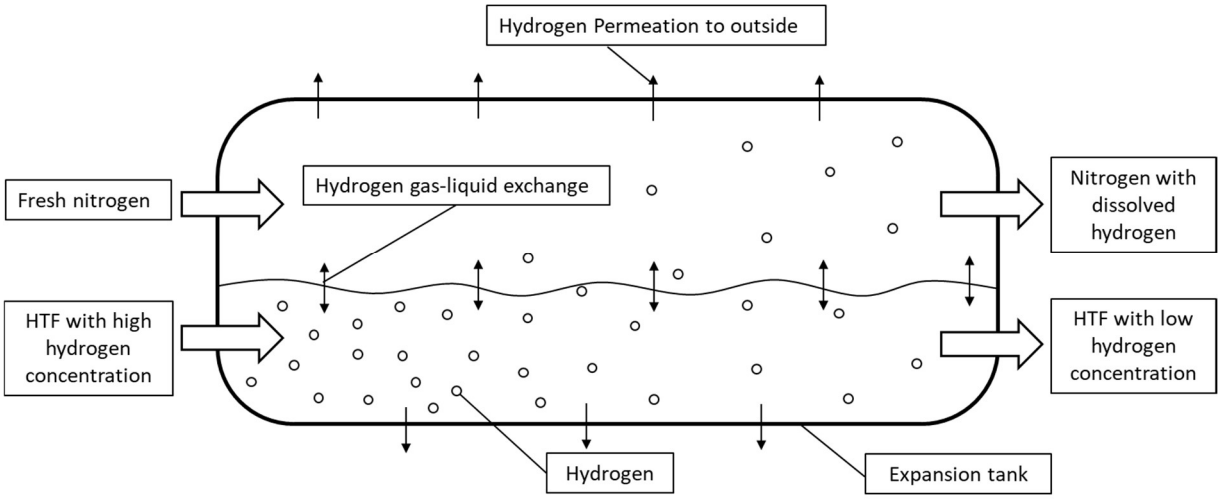

Figure 12: Hydrogen removal from HTF by flushing expansion vessel with nitrogen. Source: modified, following (Glatzmaier, 2010))

A drawback of the hydrogen removal through the expansion vessel is that the relatively small contact area of the liquid and gas phase limits the hydrogen transfer from the liquid to the gas phase. Thus,

according to Lang et al. (2017) the maximum allowable hydrogen concentration of 1 ppb requested by the receiver manufacturers cannot be reached. According to Jung and Spenke (2022) hydrogen concentrations below 100 µmol/kg, which is still far above the limit of 8 µmol/kg, can be typically found in parabolic trough plants with regular nitrogen venting. To improve the hydrogen removal by flushing the expansion vessel the surface area between liquid and gas phase could be extended by releasing gas bubbles from the head space gas through a diffusor on the bottom of the expansion tank (Beckers & Glatzmaier, 2018b). Further problems regarding the hydrogen removal through expansion vessel venting are that the additional nitrogen usage increases operating costs, brings impurities such as oxygen into the HTF and requires additional energy as it enters the expansion vessel in a cold state (Lang et al., 2017).

Glatzmaier patented a method to remove hydrogen from the vapor phase with a proton exchange membrane with a lower additional nitrogen requirement [4950](50)[50][50][50][50][50][50][50]. A hydrogen sensing and separation unit using a palladium/silver alloy membrane was installed at the Nevada Solar One power plant in 2020, but the performance of the hydrogen mitigation process still needs to be determined (Glatzmaier & Beckers, 2022). According to Lang et al. (2017) the use of a proton exchange membrane is economically disadvantageous due to its low temperature and pressure resistance and the resulting required energy intensive temperature and pressure conversion.

Lang, Belkheir et al. suggested a 2-stage process in which the hydrogen is first transfered from the liquid HTF to a vapor phase by a stripper, a flash drum or a bubble column and then removed from the vapor by a catalytic oxidation unit, a membrane unit, or an absorption unit. Even though their simulations results stated an economic benefit over frequent receiver replacement the mentioned method needs to be confirmed by physical testing (Lang et al., 2017).

Overall, no validated selective hydrogen removal method or standard for off-line analyses is available. But with the already existing techniques and components, such as nitrogen exchange, extremely high hydrogen levels could be avoided (Jung et al., 2019).

2.8 Hydrogen back-permeation from HCE to HTF

According to Fick´s first law the diffusion flux J is proportional to the negative of the concentration gradient: $J = -D\frac{\mathrm{d}c}{\mathrm{d}x}$ (Orvalho, 2009). Thus, if the hydrogen partial pressure inside the HTF is lowered, due to efficient hydrogen reduction or HTFs with low hydrogen formation, below the hydrogen pressure in the receivers' annular gap, the concentration gradient and the direction of the permeation reverse and hydrogen is transported out of the annulus into the HTF. Thus, the hydrogen pressure inside and the heat losses of receivers with hydrogen accumulation could be reduced and the plant output could be restored to its original design capacity (Beckers & Glatzmaier, 2018a; Glatzmaier, Cable, & Newmarker, 2017).

To demonstrate hydrogen back-permeation Glatzmaier, Cable and Newmarker (2017) acquired a used HCE with high heat losses due to hydrogen accumulation from a commercial plant and heated it in a laboratory without an HTF to the tubes operating temperature of 380 °C to 390 °C. After several days of heating for 8 hours each day they measured the heat losses for 300 °C, 350 °C and 380 °C. Figure 13 shows that the heat losses are clearly decreasing the more days the tubes were heated.

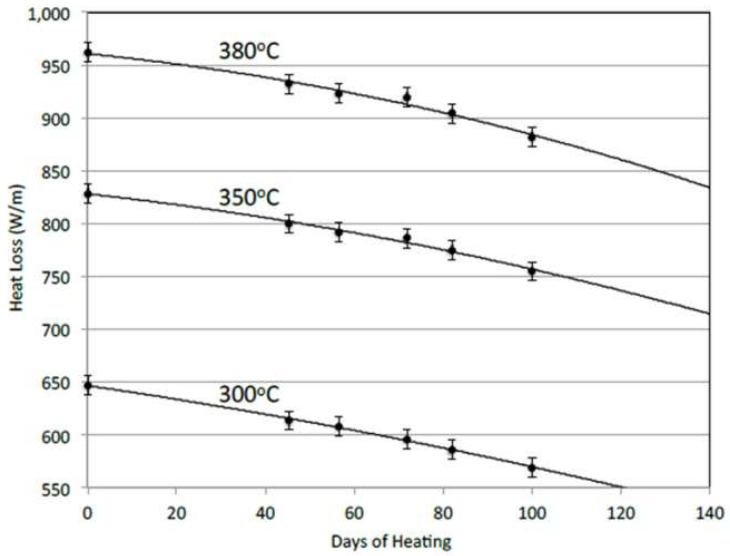

Figure 13: Receivers heat loss reduction after heating (Glatzmaier, Cable, & Newmarker, 2017)

The heat losses at 380 °C receiver temperature decreased around 8 % from an initial value of 960 W/m to 880 W/m after 100 days of heating, similar reductions were measured for 350 °C and 300 °C. As illustrated in Figure 14 these heat loss reductions equal 13 % to 17 % of the total reduction required to restore the receiver's original performance.

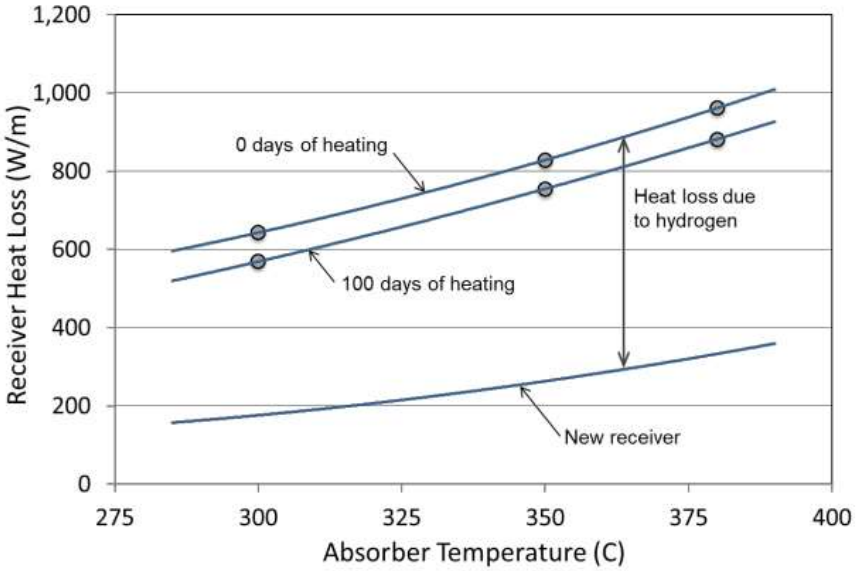

Figure 14: Heat loss of used and heated receiver in comparison to new receiver (Glatzmaier, 2020)

Hydrogen partial pressure measurements of the heated receivers showed that after 120 days of heating the hydrogen partial pressure significantly decreased from an initial value of 9.3 mbar to 1.3 mbar. According to Glatzmaier (2020) these tests demonstrate that heating of the receiver at its nominal operating temperature caused hydrogen to back-permeate out of the receiver annulus through the absorber.

The laboratory tests of Glatzmaier, Cable and Newmarker clearly show the possibility of hydrogen removal by back-permeation through the receiver tube to increase the receiver performance (Glatzmaier, 2020). However, back-permeation to an HTF has not been demonstrated yet.

3. Experimental Setup

3.1 Purpose of experiment

The objective of the experiment is evaluating the replacement of the most commonly used HTF DPO/BP with a silicone based HTF in operating power plants. The evaluation should be carried out in terms of the medium-term reduction of thermal losses of receiver tubes with hydrogen contamination. The heat loss reduction should be achieved through hydrogen mitigation from the receivers' annuli by back-permeation into HELISOL® XLP. Also, other permeation processes of hydrogen to the atmosphere through pipes, bellows or other components might occur. As the experiment is conducted with a field test facility the feasibility of hydrogen back-permeation during operation of a parabolic trough collector will be demonstrated. In a second step, hydrogen removal from the HTF will be performed by dispersing the hydrogen into a nitrogen filled expansion vessel, which is frequently vented to the atmosphere.

3.2 KONTAS facility

KONTAS (**KO**nzentrator **T**eststand **A**lmeria **S**panien) comprises a PTC module with an attached pumping, heating and cooling unit mounted on a rotatable platform. It is installed at the Plataforma Solar de Almería (PSA, owned and operated by Centro de Investigaciones Energéticas, Medioambientales y Tecnológicas (CIEMAT)) in Almería, Spain.

Figure 15: KONTAS facility at the Plataforma Solar de Almería, Spain (owned and operated by CIEMAT)

KONTAS is equipped with control and measuring technology for qualification of PTCs, components and HTFs. The two-axis tracking and the broad range of adjustable mass flow and fluid temperature enables testing and evaluating at various operating conditions. The currently installed PTC is a 12 m long Skal-ET with 5.8 m of aperture width developed by the FLAGSOL GmbH. The heating and cooling unit (HCU) pumps, heats or cools the HTF depending on the desired operating conditions. Additionally, to the HCEs in the PTC, a bypass at the side of the rotatable platform with three HCEs was added (See Figure 16). An Expansion tank with a pressurized nitrogen gas blanket is part of the HCU. Table 1 shows the main characteristics and the operation range of KONTAS.

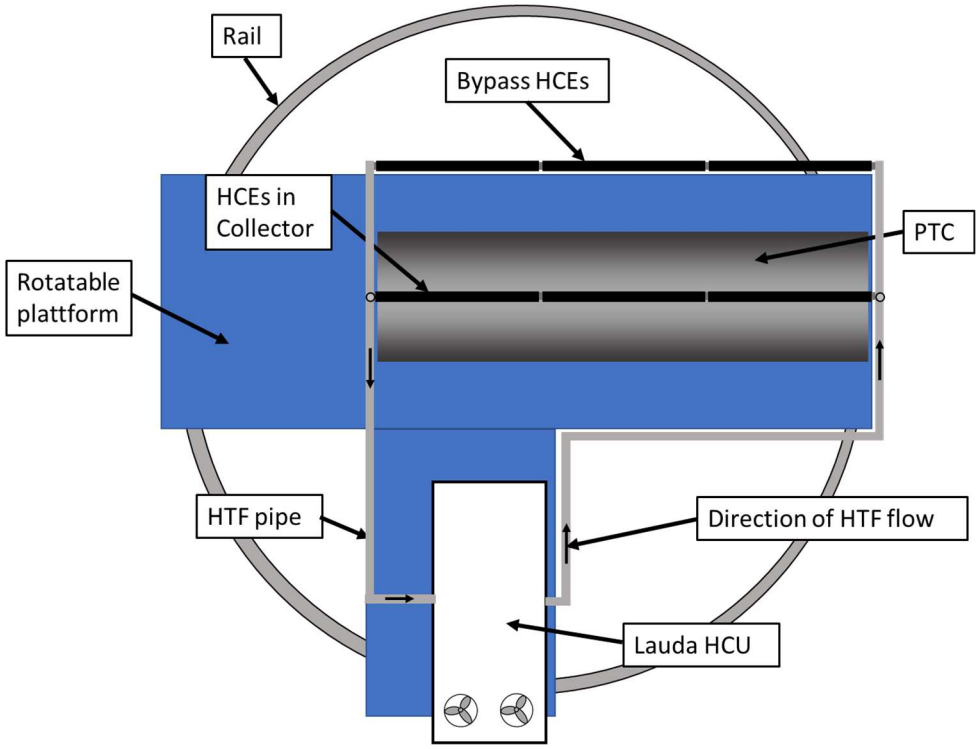

Figure 16: structure of KONTAS

Table 1: KONTAS general characteristics and design operation range

KONTAS			
PTC model:	Skal ET	Electric heating capacity:	54 kW (2x27 kW)
PTC length x aperture width:	12 m x 5,8m	Cooling capacity (currently disabled):	100 kW @ 10°C ambient Temp.
PTC aperture area:	68,125 m²	Pump capacity:	22 m³/h @ 3,5 bar
Azimuth tracking:	77° to 417°	Mass flow range:	0,5 kg/s to 5 kg/s
Elevation tracking:	-24° to 174,5°	Temperature range:	20 °C to 400 °C
Volume Expansion Tank:	750 L	Max. absolute pressure until response of safety valve:	16 bar_a

3.3 Adaption of KONTAS for back-permeation test

In this section, modifications to KONTAS to prepare the HCE hydrogen mitigation experiment are described. Changes explained in Sections 3.3.1 and 3.3.3 have been planned and mainly executed prior to this work, while those of Section 3.3.2 and 3.3.4 are part of this thesis.

3.3.1 Installation of hydrogen filled HCEs

For the experimental investigation of hydrogen reduction in PTC receivers by back-permeation numerous adjustments were made at KONTAS. The HCEs in the collector were replaced with second generation SCHOTT® PTR70 HCEs. These HCEs have been previously filled with hydrogen by DLR until the getters were saturated and 1 mbar of hydrogen pressure was reached in the annuli. To verify the uniform filling with hydrogen the thermal losses of all three HCEs were measured at CIEMAT´s HEATREC test bench (Márquez et al., 2016) before and after the hydrogen infiltration. As expected

the heat losses of all three HCEs, which were measured at absorber tube temperatures of 100, 200, 300, 350 and 400°C significantly increased after filling with hydrogen. At 400 °C the heat losses increased four-fold from original 210 … 230 W/m to 796 … 867 W/m with 1 mbar hydrogen. The measured increase of heat losses is in accordance with the measurements of Burkholder and Kutscher (2009) and Lang et al. (2017) explained in Chapter 2.5. As the difference between the heat losses of the three HCEs at each temperature is below 10 % it is verified that the HCEs contain a similar pressure of hydrogen in their annuli.

3.3.2 Doting of HELISOL® XLP with DPO/BP

To simulate the HTF composition of a power plant after a changeover from DPO/BP to a silicone based HTF, KONTAS was filled with HELISOL® XLP and doped with 2 wt.% of used VP-1 from the Andasol 3 PTC power plant. The share of 2 wt.% was selected based on the determined depuration rate after an HTF changeover at the PROMETEO test facility. PROMETEO consists of two rows of a parabolic trough collectors and it´s attached components such as an expansion tank and pumps. At PROMETEO the fraction of remaining HTF was investigated with radiation extinction tests after the HTF was changed from Syltherm™ 800 to HELISOL® 5A. There, 1 wt.% – 2 wt.% of the previous HTF remained in the system even though it was cleaned with purified, compressed air (Jung et al., 2018). The share of the remaining HTF after a changeover in a power plant was estimated to the upper end, thus to 2 wt.%.

3.3.3 Sampling, recirculation and venting system

An HTF recirculation line for mixing the HTF and to transfer hydrogen to the gas phase of the expansion tank was added to KONTAS. With an installed venting line, the expansion vessels gas phase can be released to the atmosphere. The objective of the venting is to remove hydrogen from the expansion vessel to maintain a hydrogen concentration in the HTF as low as possible. A low hydrogen concentration in the HTF is necessary to enable hydrogen back-permeation from the receivers' annulus to the HTF. Furthermore, an HTF sampling station to take hot and pressurized HTF samples to enable remote analyses of the HTF's hydrogen concentration was installed at KONTAS. Figure 17 shows the schematic structure of the installed components.

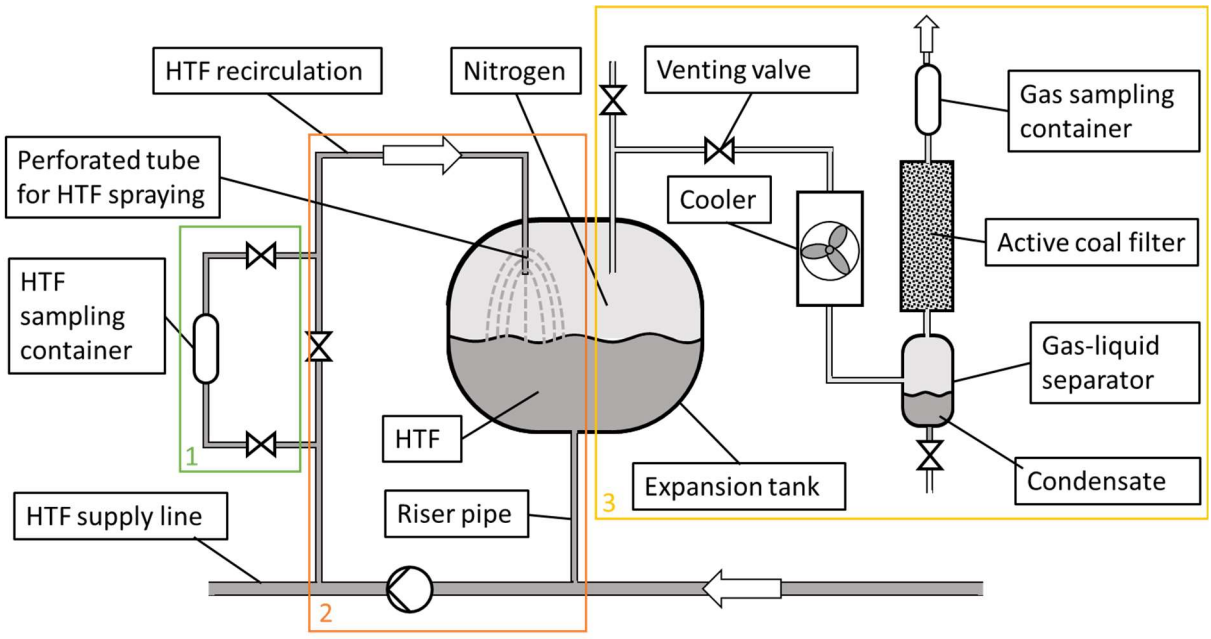

Figure 17: Schematic structure of HTF sampling station (1), HTF recirculation (2) and gas venting lines (3) at KONTAS

In the HTF sampling station (Figure 17 (1)) a share of the HTF flow from the recirculation pipe is drawn off and lead through two nitrogen-filled sampling containers, which are, thus, filled with HTF at operating pressure and temperature. The sampling containers are closed firmly and afterwards removed from the sampling station and the content is analyzed in the lab to determine its hydrogen concentration.

The HTF recirculation line (Figure 17 (2)) draws off a fraction of the HTF mass flow from the PTCs main feed line and sprays it through a perforated tube directly into the nitrogen filled gas space of the expansion vessel. The objective of the HTF recirculation and spraying is to enhance the hydrogen transfer from the circulating HTF to the gas phase inside the expansion vessel.

To remove the gas phase with the accumulated hydrogen from the expansion vessel a gas venting line (Figure 17 (3)) was added. When the venting valve is opened the nitrogen with the diffused gases including hydrogen leaves the expansion vessel through a cooler, a gas-liquid separator and an active coal filter towards the atmosphere. The gas-liquid separator is used to hold back low boiling fractions of HELISOL® XLP and can be emptied through a valve at the bottom. After the venting fresh nitrogen is fed into the expansion vessel to restore the operating system pressure and to take up hydrogen through equilibration with the hydrogen in the HTF.

Figure 18 shows a photo of the implemented HTF sampling station, HTF recirculation and nitrogen venting system installed at KONTAS.

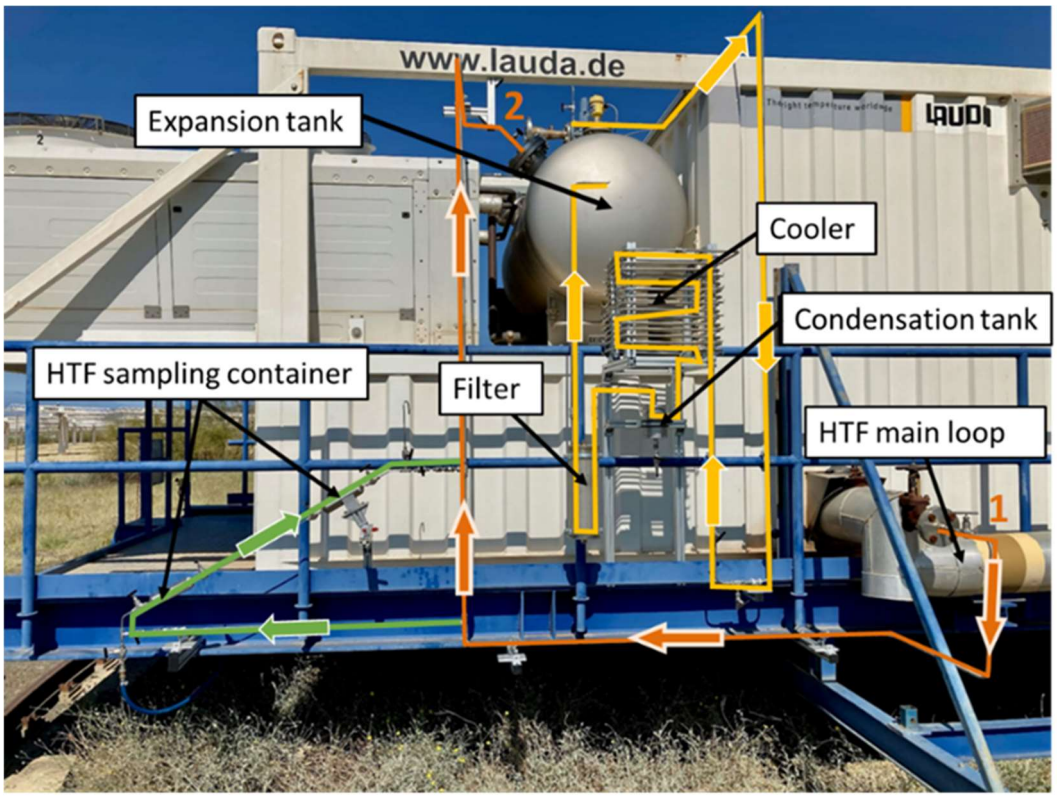

Figure 18: Installed HTF sampling station (green), HTF recirculation (orange) and gas venting lines (yellow) installed at KONTAS (prior to installation of insulation)

3.3.4 HCE Temperature Measurements

Hydrogen accumulation in the vacuum annuli can significantly increase the HCEs glass envelope temperatures and thus the heat losses during operation. Thus, measuring the glass envelope temperatures at KONTAS during operation could give a rough indication on the condition of the HCEs and long-term changes of hydrogen partial pressure might be detected. For the temperature measurement at KONTAS, thermocouples of type K, generally known as nickel-chromium-nickel thermocouples were applied. The accuracy of these thermocouples, class 2, in the temperature range of -40 °C to 333 °C is ±2.5 °C (TC Mess- und Regeltechnik GmbH, 2024). The attachment of the thermocouples to the HCEs was done by taping the thermocouples parallel to the receiver's axis to the upper side of the glass envelope (see Figure 19). The upper side was selected to prevent the thermocouples from heating up by the concentrated solar light reflection from the collector. For better heat transfer from the glass surface to the thermocouple, a thermo-conductive paste was applied at the sensor tip of the jacket tube. For redundancy two thermocouples were installed next to each other at each HCE in the collector as well as on the HCEs of the bypass.

Figure 19: Attachment of thermocouples to glass envelope of HCE

As shown in the schematic top view of KONTAS in Figure 20 the thermocouples are connected to two ALMEMO® 2890 data loggers, which themselves are connected via a bus system to a power supply unit and a laptop for data acquisition and synchronization of the data loggers. Both dataloggers were put in waterproof cases, the one for the bypass HCEs was mounted on the side of the base platform while the datalogger for the HCEs in the collector was installed on the steel structure on the backside of the PTC.

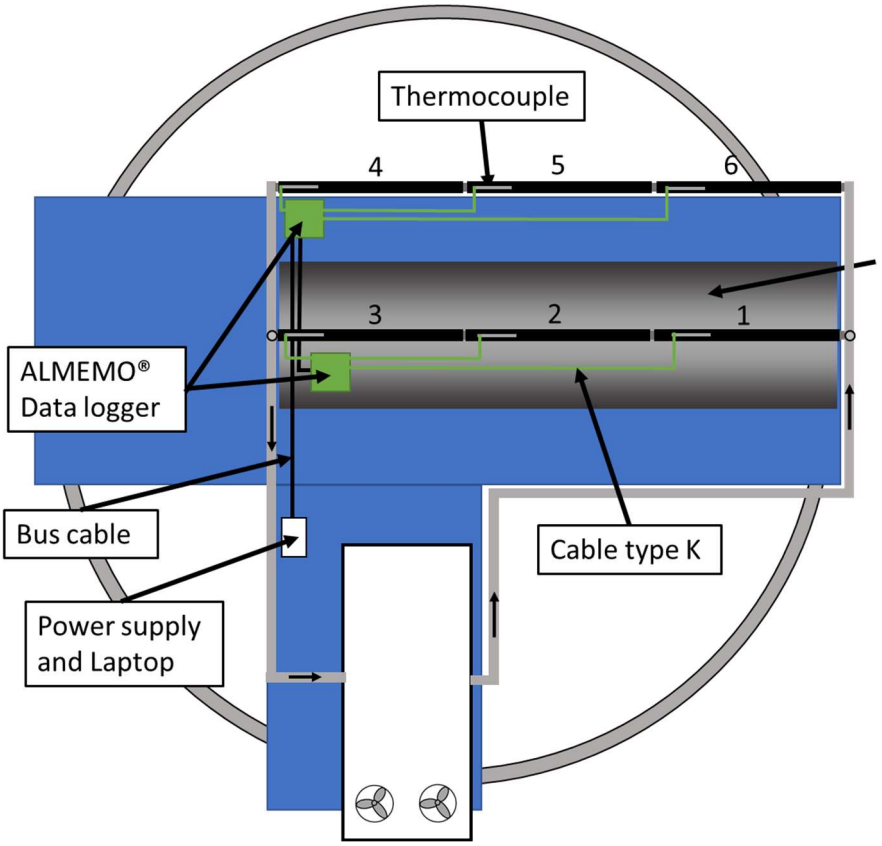

Figure 20: Schematic structure of HCE temperature measurement system at KONTAS

4. Development of operation and data evaluation strategies

4.1 Operation parameters

The operating conditions of KONTAS were selected to imitate operating conditions in power plants switching their HTF from DPO/BP to HELISOL® XLP. HELISOL® XLP itself can withstand temperatures of 425 °C and above (C. Hilgert (DLR), 2021; Wacker Chemie AG, 2020), but most important components in operating power plants such as HTF pumps, HCEs, headers & piping, ball joints, evaporators, expansion tanks, sensors and valves are designed for a maximum temperature of 400 °C (Wehner, 2022). Accordingly, the maximum operation temperature of a power plant switching to HELISOL® XLP could be slightly increased from 393 °C to 400 °C without major changes to the hardware. To simulate this new operation conditions an operating temperature of 400 °C was selected for the experiment. To operate above the vapor pressure of HELISOL® XLP of 10.3 bar at 400 °C (Wacker Chemie AG, 2020) and below the response of KONTAS safety valve opening at 16 bar, the operation pressure was set to an absolute pressure of 13 bar.

KONTAS is operated at the maximum achievable HTF mass flow of around 5 kg/s. This maximizes the HTF recirculation mass flow which improves hydrogen dispersion and permeation inside the receiver tube and increases the hydrogen transfer to the gas phase of the expansion vessel. To improve the hydrogen transfer from the HTF to the gas phase of the expansion tank, the recirculation, which draws off and sprays a fraction of the main HTF flow into the expansion tank, is open during nominal operation. During the ventilation procedure the recirculation is closed.

Glatzmaier, Cable and Newmarker (2017) conducted an experiment in which they heated hydrogen contaminated receivers for 100 days with 8 hours per day. They achieved a thermal loss reduction of

13 % to 17 % of the reduction to restore the receiver's original performance. This partial reduction shows that the hydrogen mitigation in the receiver by back-permeation is a slow process. At KONTAS HTF circulates through the receivers while in the back-permeation experiment of Glatzmaier, Cable and Newmarker (2017) air was inside the receiver tube. Due to hydrogen formation inside the HTF, back-permeation and intermittent venting the hydrogen partial pressure of the HTF inside the receiver tubes at KONTAS is expected to be larger than the hydrogen pressure of ambient air. Thus, the increased hydrogen partial pressure inside the receiver tube will probably decrease the hydrogen partial pressure difference between the vacuum annulus and the HTF, which is the driving force of back-permeation. So, the permeation process at KONTAS or in a power plant is expected to be slower than in the described laboratory experiment. The operation time for the back-permeation tests at KONTAS was therefore set to 3000 h.

KONTAS is operated 24/7 to reduce the required days for the experiment. The daytime solar operation is extended by electrically heated and autonomous operation during nighttime, cloudy days, and maintenance or malfunctioning of the tracking mechanism.

Table 2: Operation parameter of KONTAS

Nominal operation parameters	
Heat Transfer Fluid:	HELISOL® XLP with 2 wt.% used VP-1
Setpoint Temperature of heating and cooling unit:	400 °C
Main mass flow:	5 kg/s
HTF recirculation	open
Pressure:	13 bar_a
Time period:	3000 h
Operating times:	24/7
Heating mode:	Solar thermal / electric

4.2 Venting and sampling strategy

4.2.1 Effect of venting temperature on formation of condensate

To discharge the expansion vessel's gas phase with the dissolved hydrogen, the head gas can be released to the atmosphere by opening the valves of the venting system consisting of cooler, condensate separator andactive coal filter (See chapter 3.3.3). The head gas phase not only consists of nitrogen and hydrogen, but also low boiling components of the HTF with different boiling temperatures such as Hexamethyl-disiloxane ($C_6 H_{18} O_1 Si_2$), Hexamethyl-cyclotrisiloxane ($C_6 H_{18} O_3 Si_3$) and Octamethyl-cyclotetrasiloxane ($C_8 H_{24} O_4 Si_4$) with a boiling point of 100 °C, 135 °C respectively 175 °C can be formed. Thus, the venting temperature has an impact on the composition as well as on the amount of condensate formed during the venting.

To investigate the amount of condensate occurring in the venting process, the amount of condensate for venting temperatures of 50 °C to 200 °C was measured. The venting procedure for the condensation measurement consists of the following steps:

1. The HTF recirculation pipe from the main HTF flow to the expansion tank is opened
2. The pump is set to its maximum mass flow of around 5 kg/s and the electric HTF heater setpoint is set to the desired venting temperature
3. When the desired HTF temperature is reached in the main loop as well as in the expansion tank, the pressure in the expansion tank is set to 6 bar

4. The operation is continued at constant temperature for 10 min
5. The recirculation is closed and the HTF is held at temperature for another 10 min
6. The gas phase of the expansion vessel is vented from 6 bar to 3.5 bar absolute pressure
7. The condensate formed during the venting is taken from the condensate separator and weighted on a digital scale.

As the HTF expands at higher temperatures the HTF fill level in the expansion tank increases with the temperature. To better compare the amount of condensate at different temperatures the amount of vented nitrogen and the ratio of condensation per vented nitrogen mass were calculated.

With the assumption of an ideal gas the mass of nitrogen, m_{N_2}, inside the expansion vessel was calculated from solving the ideal gas equation $pV = nRT$ with $n = m/M$ for m:

$$m_{\mathrm{N}_2} = \frac{p_{\text{expansion vessel}} * V_{\mathrm{N}_2} * M_{\mathrm{N}_2}}{R * T_{\text{expansion tank}}} .$$

$p_{expansion\ vessel}$ is the pressure in the expansion vessel, V_{N_2} is the volume of the gas phase with the assumption that nitrogen makes up almost all of the gas phase and is calculated by $V_{\mathrm{N}_2} = \mathrm{V}_{\text{expansion tank}} * (1 - F)$ with F being the HTF fill level of the expansion tank. Furthermore, $M_{\mathrm{N}_2} = 28{,}0134\ \mathrm{g/mol}$ is the molar mass of nitrogen, $R = 8.4145\ \frac{\mathrm{J}}{\mathrm{mol} * \mathrm{K}}$ is the ideal gas constant and $T_{\text{expansion tank}}$ is the temperature of the gas phase in the expansion tank.

To calculate the mass of vented nitrogen, the mass of nitrogen after the ventilation was deducted from the nitrogen mass before the ventilation:

$$m_{\mathrm{N}_{2,\text{vented}}} = m_{\mathrm{N}_{2,\ \text{before venting}}} - m_{\mathrm{N}_{2,\ \text{after venting}}}$$

Which results with all variables inserted in:

$$m_{N_{2,vented}} = \frac{p_{\text{before venting}} * \mathrm{V}_{\text{expansion tank}} * (1-F) * M_{N_2}}{R * T_{\text{expansion tank}}} - \frac{p_{\text{after venting}} * \mathrm{V}_{\text{expansion tank}} * (1-F) * M_{\mathrm{N}_2}}{R * T_{\text{expansion tank}}}$$

$$= \frac{\mathrm{V}_{\text{expansion tank}} * (1-F) * M_{\mathrm{N}_2}}{R * T_{\text{expansion tank}}} * (p_{\text{before venting}} - p_{\text{after venting}})$$

Table 3 shows the results of the condensate measurements for different temperatures as well as the calculated amount of vented nitrogen.

Table 3: Results of condensate measurement for venting temperatures of 50 °C to 200 °C

Temperature [°C]	Amount of condensate [g]	HTF fill level in expansion tank F	Start pressure [bar_a]	End pressure [bar_a]	Amount of vented nitrogen [g]	Mass of condensate per mass of vented nitrogen [g/g]
50	0	31,5 %	6	3,5	1 340	0.0
75	0	33,9 %	6	3,5	1 200	0.0
100	2	36,2 %	5,9	3,5	1 040	0.002
125	94	37,7 %	6	3,5	990	0.095
150	155	39,7 %	6	3,5	900	0.172
175	433	41,6 %	6,1	3,5	860	0.505
200	620	43,5 %	5,9	3,5	720	0.856

It can be clearly seen that the amount of condensate significantly increases for higher temperatures. Due to expansion of the HTF and the smaller density of the gas phase at higher temperatures the amount of vented nitrogen for the same pressure difference decreases. So, to better compare the amount of condensate the ratio of amount of condensate per vented nitrogen mass was calculated. This ratio (right column of Table 3) is visualized graphically in Figure 21.

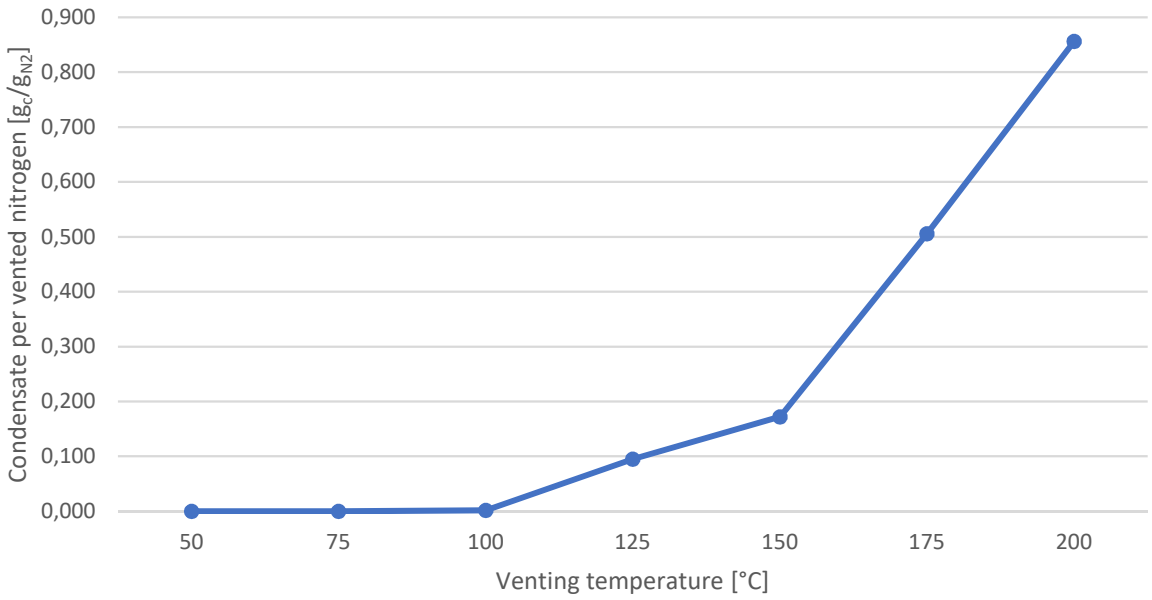

Figure 21: Ratio of condensation mass per vented nitrogen mass

It can be seen that below 100 °C no condensate was found, between 100 °C and 150 °C the amount of condensate per vented nitrogen mass is growing linear up to a share of 0.172 g_c / g_{N2}. Above 150 °C the amount of condensate per vented nitrogen mass increases noticeable steeper up to 0.856 g_c / g_{N2} at 200 °C. Thus, at 200 °C almost as much condensate is formed as nitrogen in vented. To further investigate the condensate´s composition, condensate samples were sent to WACKER CHEMIE AG for analyses, but at the time of this thesis the results are not yet received.

4.2.2 Venting procedure during operation

A frequent venting with withdrawal of large amounts of condensation might affect the composition, characteristics and degradation rate of the HTF, so venting at lower temperatures with less condensate would be preferred. But due to the injection of hot HTF from the main loop through the recirculation pipe the expansion tank heats up to around 370 °C during nominal operation. The cooldown time of the expansion tank to reach low venting temperatures is contrary to the objective of frequent venting and HTF recirculation, which are important for the hydrogen transfer from the HTF to the atmosphere. During test operation of KONTAS is was recognized that a cooldown to 150 °C, which takes around 16 h to 18 h, is from an operator's perspective the most feasible and repeatable option as it is possible overnight, only moderate amounts of condensate are formed and it leaves time during working hours to perform the ventilation and recirculation.

During cooldown from 370 °C to 150 °C expansion tank temperature the pressure decreases from the nominal pressure of 13 bar to 4 bar. For the venting process the lower pressure limit was selected to 1,5 bar, to always maintain a pressure difference between the expansion tank and the atmosphere to prevent oxygen, water and other impurities from the atmosphere to enter the system. So, the venting is performed from 4 bar to 1,5 bar. With the assumption of only nitrogen in the gas phase,

which forms an ideal gas, a constant expansion tank temperature and a constant gas phase volume during venting, the share of vented nitrogen mass can be calculated. The ideal gas equation

$$pV = nRT \text{ with } n = \frac{m}{M}$$

is solved for the volume of the gas phase in the expansion tank and put on a level before and after venting:

$$V_{\text{gas phase}} = V_{\text{gas phase,before venting}} = \frac{m_{\text{before venting}} * R * T}{M_{\text{N}_2} * p_{\text{before venting}}}$$

$$= V_{\text{gas phase,after venting}} = \frac{m_{\text{after venting}} * R * T}{M_{N_2} * p_{\text{after venting}}}.$$

With R, T and M_{N_2} being constant follows the equation:

$$\frac{m_{\text{after venting}}}{m_{\text{before venting}}} = \frac{p_{\text{after venting}}}{p_{\text{before venting}}}.$$

The share of vented gas phase can thus be calculated by:

$$1 - \frac{m_{\text{after venting}}}{m_{\text{before venting}}} = 1 - \frac{p_{\text{after venting}}}{p_{\text{before venting}}}.$$

So, when venting from 4 bar to 1,5 bar, around 62,5 % of the gas phase are vented. Assuming, furthermore, a uniform distributed of hydrogen in the gas phase, 62,5% of the hydrogen in the gas phase is vented. To improve the hydrogen mitigation by increasing the share of the gas phase which is vented, fresh nitrogen is filled in to restore the pressure back to 4 bar and the venting is repeated.

For an ideal mixture and the same assumptions and parameters as in the first venting the share of exchanged gas phase after venting twice is therefore:

$$1 - \left(\frac{m_{\text{after venting}}}{m_{\text{before venting}}}\right)^2 = 1 - \left(\frac{p_{\text{after venting}}}{p_{\text{before venting}}}\right)^2$$

The repeating of the venting for a second times increases the share of the gas exchange and the share of removed hydrogen from around 62,5 % to approximately 86 %.

After the venting, fresh nitrogen is filled back in to restore the pressure of 4 bar and the HTF recirculation is reopened. Thus, when heating up again to 370 °C the pressure reaches again 13 bar operation pressure. If the pressure would be directly increased to 13 bar by filling nitrogen to the expansion tank at a tank temperature of 150 °C, the heat up could lead to an increase of pressure and an uncontrolled emission of nitrogen through the safety valve (opening at 16 bar).

Considering the measurement of condensate for different venting temperatures, the venting pressure and practical aspects such as working hours of the operators the venting procedure can be concluded to the following steps (with 0. being the initial situation):

0. KONTAS is operated in nominal operation condition (HTF temperature in main loop is at 400° C, expansion tank at 370 °C, recirculation is open)
1. Close the recirculation valve
2. Expansion tank cools town to 150 °C (pressure decreases to 4 bar)
3. Turn off Lauda, to prevent cavitation of the pump caused by low pressure during venting
4. Vent the expansion vessel from 4 bar to 1,5 bar

5. refill fresh nitrogen to 4 bar
6. vent again from 4 bar to 1,5 bar
7. refill fresh nitrogen to 4 bar
8. Restart Lauda
9. reopen recirculation valve and continue with 0.

4.2.3 Venting control and frequency

To investigate the effectiveness of the described venting procedure regarding the mitigation of hydrogen in the HTF, samples were taken before and after a venting, which was performed after 24 h at nominal operation conditions.

Before sampling, the HTF is mixed for 2 hours to reach a homogenous composition to allow for a representative sampling. The first step of the sampling process is to install two empty sampling containers in the sampling station shown in Figure 22, which are then flushed with nitrogen to remove air, water and other impurities. Afterwards the valves separating the sampling station from the recirculation flow are opened and HTF flows through the sampling containers. Once the sampling container reached a steady temperature, which was measured with a contact thermometer, the valves of the containers were closed.

Figure 22: Close up of the HTF sampling station (prior to the installation of thermal insulation)

By this method the samples of mixed HTF can be taken at operating pressure and temperature to have the same condition and composition of the HTF in the main loop. After cooldown of the sampling station the containers were removed, labeled and sent to a DLR lab in Cologne for offline-analysis of hydrogen concentration with pressure measurement and gas chromatography. Table 4 shows the laboratory results of the hydrogen concentration in the gas phase of the HTF samples before and after venting.

Table 4: Concentrations in the HTF samples' gas phase before and after venting

	Weight			Concentrations					
Sample label	full [g]	empty [g]	m_{HTF} [g]	c_{H2} [ppm]	c_{CH4} [ppm]	c_{C2H6} [ppm]	c_{CO} [ppm]	c_{CO2} [ppm]	c_{N2} [ppm]
PSA KONTAS, HELISOL XLP, @400°C 9,8bar, **Before venting**	1541,4	1359,5	182	1970	10 252	11	3	64	987 700
	1522	1352	170	1875	10 677	12	42	57	987 337
PSA KONTAS, HELISOL XLP, @392°C 10,5bar, **After venting**	1537,8	1357	180,8	1102	4483	8	17	57	994 335
	1527,4	1356,6	170,8	1137	4614	9	19	62	994 101

The laboratory analysis of the HTF samples show a significant reduction of the hydrogen concentration in the gas phase of the HTF. From an initial value of 1970 ppm in the first, respectively 1875 ppm in the second sampling container the hydrogen concentration was reduced through the venting by around 40 % to 1102 ppm in the first and 1137 ppm in the second sampling container (Table 4). Also, the concentration of methane (CH_4) was drastically reduced, but due to its larger molecule size it is less likely to permeate into the vacuum anulus, and is therefore less important for the evaluation of the venting.

Internal assumptions of DLR state that the current hydrogen concentration and the resulting partial pressure is too high to cause hydrogen back-permeation and estimate that a hydrogen concentration well below 100 ppm is required to achieve hydrogen back-permeation from the vacuum annuli to the HTF. In order to further lower the hydrogen concentration, a high venting frequency is required, so the described venting procedure in 4.2.2 is scheduled to be carried out daily. This can be achieved by timing the venting procedure in a way that the most time-consuming step, the cooldown of the expansion tank (step 2) is done during the night and the more work-intensive steps are performed during the work hours of one day. Resulting the following time schedule was developed for the daily venting procedure:

Table 5: Time schedule for daily venting procedure

Step	Description	Scheduled time
0.	KONTAS is in nominal operation condition (HTF temperature in main loop is at 400° C, expansion tank at 370 °C, recirculation is open)	Around 11:00 h to 16:00 h
1.	Close the recirculation valve	At 16:00 h, end of the workday
2.	Expansion tank cools down to 150 °C (pressure decreases to 4 bar)	Takes 16-18 h, depending on weather conditions
3.	Turn off Lauda, to prevent cavitation of the pump caused by low pressure during venting	Once 150 °C is reached. (Typically, between 8:00 h and 10:00 h)
4.	Vent the expansion vessel from 4 bar to 1,5 bar	As soon as previous step is completed
5.	Refill fresh nitrogen to 4 bar	As soon as previous step is completed
6.	Vent again from 4 bar to 1,5 bar	After 10 min
7.	Refill fresh nitrogen to 4 bar	As soon as previous step is completed
8.	Restart Lauda	As soon as previous step is completed
9.	Reopen recirculation valve to go back to nominal operation	As soon as previous step is completed.

A weekly HTF sampling is planned to regularly check the hydrogen concentration in the HTF to further evaluate the effectiveness of the venting strategy. Depending on the laboratory results the venting and recirculation procedure as well as the time schedule might need to be adapted to reach higher frequencies.

4.3 Method to analyze HCE temperature data

To detect long term changes of the hydrogen partial pressure inside the HCEs the surface temperatures of the glass annuli are measured during operation of KONTAS with the temperature measurement system explained. The HCE temperatures are logged every minute and are read out from the dataloggers by the ALMEMO® Control 6.3 Software installed on the measurement laptop, which is connected to the dataloggers through the bus system. An automation script to automatically collect, unite and store the data from both dataloggers was created with “AutoHotkey”, an open-source scripting language for automation tasks on Windows. To set the HCE temperature data in relation to the operation data of KONTAS a MatLab script merges and synchronizes the KONTAS operation data with the HCE temperature data. To detect the desired long-term changes in HCE temperature the temperature data are illustrated graphically over the operation time and can be analyzed visually.

At the time of the completion of this thesis a first week of nominal operation of KONTAS was achieved in January 2024. Due to a technical fault of the elevation drive KONTAS was operated electrically and the PTC was facing north. The recorded temperatures of the HCEs in the collector, basic ambient conditions such as ambient temperature, wind speed and humidity, as well as major operational parameter of KONTAs such as the HTF temperature in the HCEs outlet are shown in Figure 23.

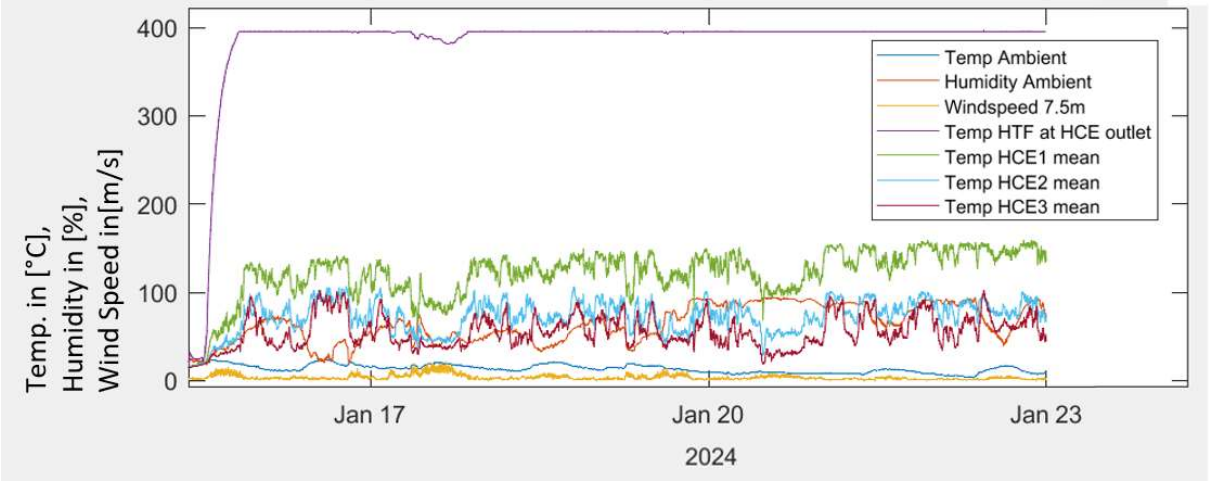

Figure 23: Graph of HCE temperatures, ambient conditions and KONTAS parameter

The temperatures of each HCE are averaged from the two thermocouples at each HCE. As the time period is relatively short and a later analyzed HTF sample showed that the hydrogen concentration in the HTF during this week probably was too high for the hydrogen to back-permeate, no reduction of the HCE temperatures is observed. But the graphical visualization can be used for a rough estimation of the effect of weather conditions on the HCE temperatures.

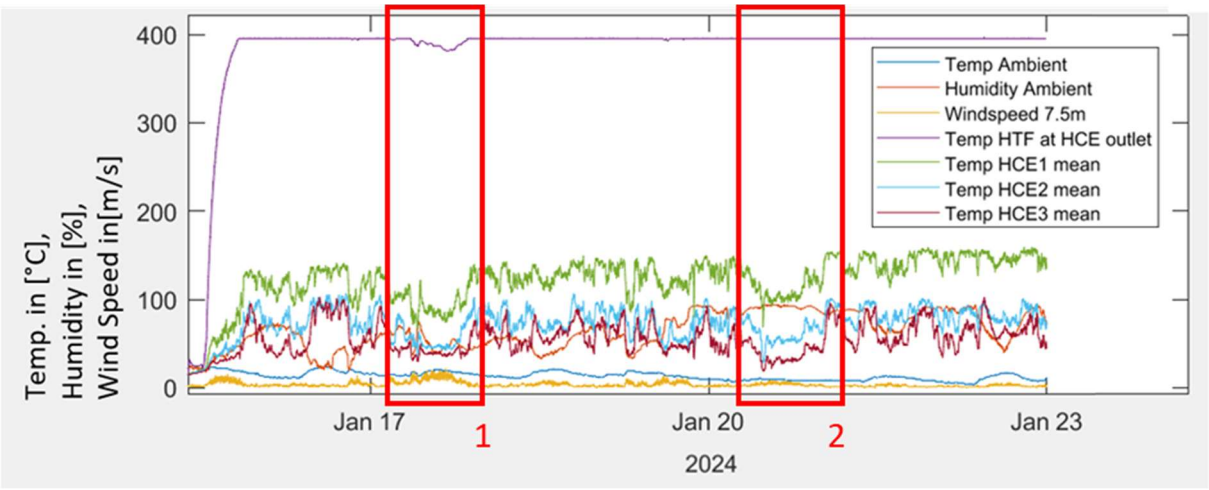

Figure 24: Effect of weather conditions on HCE temperatures

In the first marked square in Figure 24 it can be seen that the HTF temperature at the HCE outlet in the collector (purple line) fluctuates and drops from its stationary value during operation of around 397 °C to around 380 °C. Also, the HCE temperatures in the same square are lower than before and after the marked section. The reason for the reduced temperatures is that the high windspeeds of up to 22 m/s in this time period increased the convective heat losses occurring at the HCEs, as well as at other tubes and components. As not only the windspeed, but also its direction and possible turbulences or slipstreams of the PTC might have an effect on the convection at the HCEs it would be difficult to estimate the temperature of the HCEs without the wind.

In the second marked square in Figure 24 a similar reduction of HCE temperatures can be seen, even though the windspeeds are significantly lower than in the first square. It was noticed by the operators that in this time period it was raining at the PSA. It is assumed that the thereby caused wetting of the glass envelope lowered their surface temperatures due to increases heat losses. A rough indicator but not a proof to recognize rain in the graphical visualization could be the measured ambient air humidity.

As rain is not frequent at PSA, the operators could manually note if there are longer time periods with rain and consider them when looking at the long-term temperature data.

The effect of the ambient temperature is expected to have a minor influence on the long-term analysis of the HCE temperature data, because the expected HCE temperature changes if the hydrogen partial pressure can be reduced drastically are much larger than the changes of ambient temperature. According to Glatzmaier (2010) the glass annulus temperature for a receiver at 400 °C will decrease from 150 °C with 1.33 mbar of hydrogen inside the glass annulus to 50 °C without hydrogen. In the numerical study of Lei, Ren and Wang (2020) already a smaller decrease in hydrogen partial pressure from 1 mbar to 0.1 mbar caused a reduction of the HCEs glass envelope temperature of around 50 °C from around 150 °C to 100 °C.

Within this week of operation, no further effect of the weather conditions on the HCE temperatures could be specified. To facilitate the visual analyses a prefiltering of the data could be used to show only data for predefined weather or operating conditions. In Figure 25 the same time period as in Figure 23 is depicted, but only those values are shown in with the operating and weather conditions are as followed:

1. The HTF outlet temperature is above 390 °C
2. The pump mass flow is above 4 kg/s
3. The windspeed is below 3 m/s

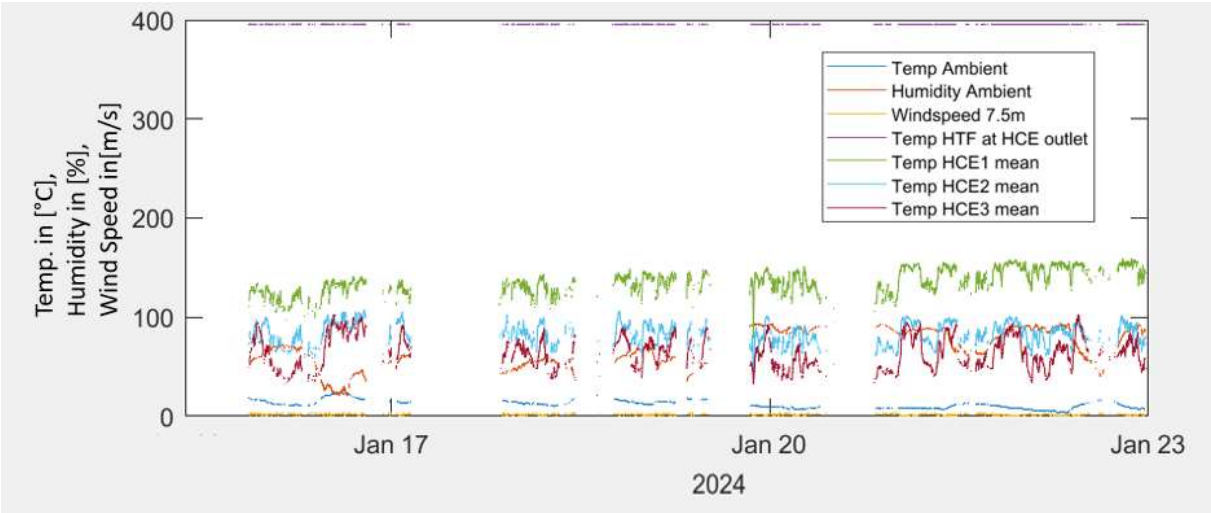

Figure 25: Graph of prefiltered data for visual analysis of HCE temperature changes

It is important to consider the effects of wind and rain on the HCE temperatures when looking at the changes of the HCE temperatures. A prefiltering as in Figure 25 could help the viewer to neglect time periods with operation or weather conditions which deviate from the standard conditions.

By looking at the HCE temperature data a big temperature difference between the three HCEs in the PTC was recognized. During operation HCE 1 is at 130 °C, while HCE 2 and HCE 3 are at around 80 °C respectively at 70 °C. As the HCEs showed similar performance in the initial heat loss laboratory tests this temperature difference was not expected. To eliminate the possible source of error of incorrectly attached thermocouples, the temperatures of the HCEs in the collector (HCE number 1,2 and 3 in Figure 26) and in the bypass (number 4, 5 and 6 in Figure 26) were measured with a ZENMUSE XT2 infrared (IR) camera drone from DJI (DJI, 2018).

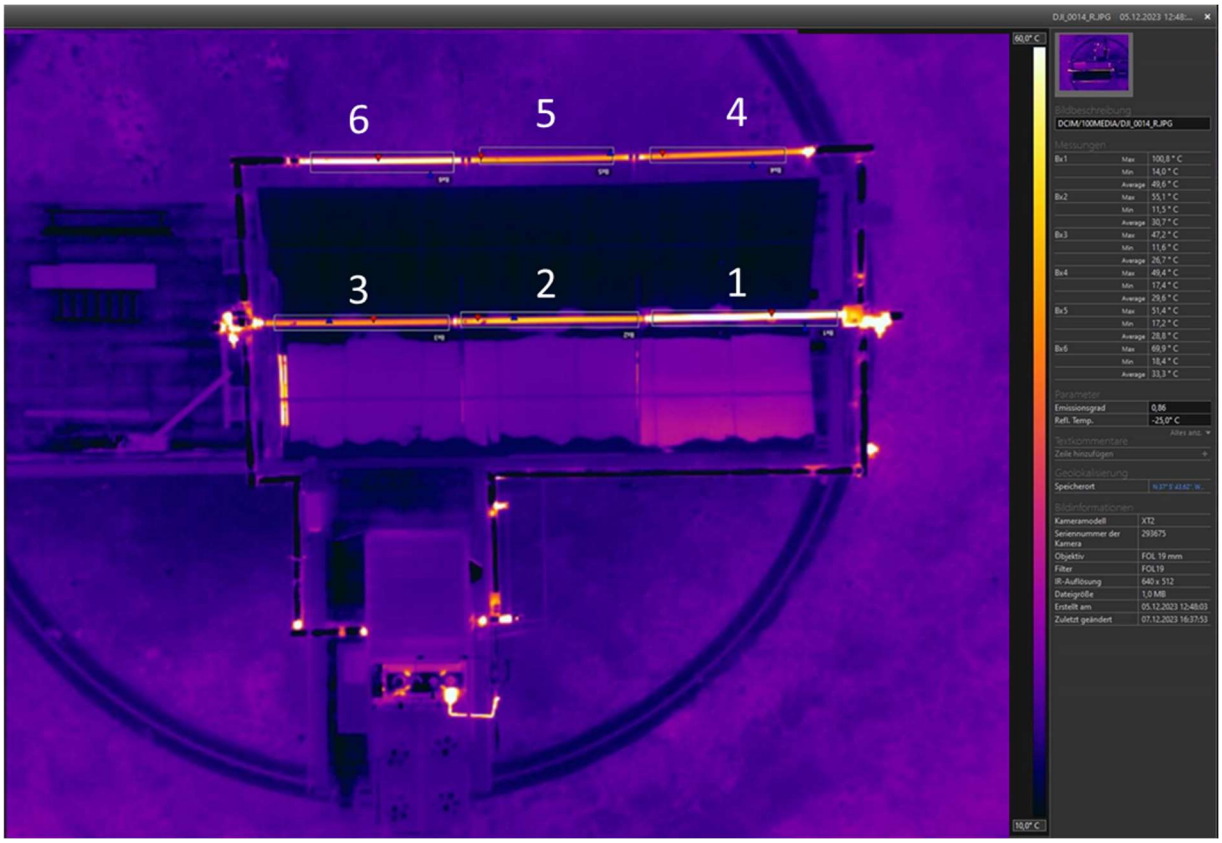

Figure 26: Infrared image of the HCE temperatures at KONTAS during operation

Table 6 contains the HCEs temperatures measured by the thermocouples as well as by the IR camera. Both thermocouples at each HCE show similar values, so both thermocouples are installed similar at each HCE. The difference of maximum 5.8 °C could be partially caused by the thermocouple's accuracy of ±2.5 °C and by slightly different sizes and orientation of the aluminum tapes covering the thermocouples. The IR measured HCE temperatures are around 25 to 35 % higher than the temperatures measured by the thermocouples. Those large differences in absolute temperatures are caused by the roughly estimated emissivity of the soiled HCEs at KONTAS. The estimated HCE glass surface emissivity of 86 % used for the processing of the IR measurement was probably overestimated as sand and other soiling might reduce the emissivity of the HCEs significantly. But as all HCEs are in similar conditions and are measured at once by the IR drone, the relation of the HCE temperatures to each other can be ascertained. The averaged thermocouple values of each HCE as well as the IR measured temperatures are divided by the maximum temperature value of each measurement method, so the hottest HCE is set to a value of 1,0 (See Table 6). Thus, the relation of the HCEs to each other can be compared independent from the absolute values. By comparing the IR measured HCE temperatures relation to the thermocouple measured relation it can be checked if the thermocouples at each HCE are installed correctly.

Table 6: Comparison of thermocouple and IR measured HCE temperatures

	HCEs in PTC			HCEs in Bypass		
HCE Nr.:	1	2	3	4	5	6
Thermocouple 1 [°C]:	129,7	76	65	67,1	66,8	91,3
Thermocouple 2 [°C]:	127,4	73,3	65,4	61,4	62,8	85,5
Thermocouple average [°C]:	128,55	74,65	65,2	64,25	64,8	88,4
IR measurement [°C]:	100,8	55,1	47,2	49,4	51,4	69,9
Relation of the HCE temperatures to each other (maximum value =1):						
Thermocouple average:	1,000	0,581	0,507	0,500	0,504	0,688
IR measurement:	1,000	0,547	0,468	0,490	0,510	0,693
absolute deviation:	0,000	0,034	0,039	0,010	-0,006	-0,006
Relative deviation in relation to IR measurement (%):	0,00%	6,23%	8,32%	1,98%	-1,14%	-0,83%

Overall the IR measurement shows that the thermocouples show the relation of the HCE temperatures with a deviation of less than 10 %. Thus, incorrectly attached thermocouples are not the reason for the measured large temperature differences of the HCEs. Due to technical issues of KONTAS, the operation was paused shortly after the observation was made and further investigation on the reason for the temperature differences was not possible yet. But even if the HCEs have different performances a long-term monitoring of each one individually might help to detect a reduction of glass surface temperatures.

5. Conclusion and Prospect

In this thesis the hardware of KONTAS was adapted for the experimental investigation of hydrogen reduction in PTC receivers by back-permeation into HELISOL® XLP. This was achieved by completing the installation of the HTF recirculation line, venting line and HTF sampling station. Also, a temperature measurement system was planned and installed on the HCEs' glass envelopes to quantify the desired loss of glass envelope surface temperatures during operation in case of an effective hydrogen reduction. To imitate the conditions of a PTC power plant changing its HTF from DPO/BP to a silicon based HTF, KONTAS was filled with HELISOL® XLP and doped with used VP-1. A share of 2 wt.% VP-1 was selected based on the measured depuration rate after a changeover at another DLR PTC test facility. With the same objective the operation parameters were chosen to an HTF temperature of 400 °C, a pressure of 13 bar and a mass flow of the maximum value possible at KONTAS of around 5 kg/s.

Furthermore, an expansion vessel venting strategy was developed to remove hydrogen from the HTF by exchanging the gas phase above the HTF. The objective of the venting is to maintain a hydrogen concentration in the HTF as low as possible to enable hydrogen back-permeation from the HCEs to the HTF. The first step in the development of the venting parameters was the investigation of the amount of condensate forming for different venting temperatures. It was experimentally confirmed that condensate accrues above a venting temperature of 100 °C and that the amount of condensate per vented nitrogen significantly increases with a further increase in venting temperature. Considering the working times of the operators as well as the contrary aspects of required cooldown time and the amount of condensate lost during the venting, a feasible compromise was found at an expansion vessel

temperature of 150 °C. The venting start and end pressure, which determine the share of the vented gas phase, were selected to a start pressure of 4 bar and an end pressure of 1.5 bar. It was calculated that venting twice in a row with this pressure range at 150 °C around 86 % of the gas phase are exchanged. The effectiveness of the described venting process was proofed by taking HTF samples before and after the venting. The gas chromatography analysis by DLR showed that a reduction of hydrogen concentration of 40 % from around 1900 ppm to 1100 ppm hydrogen in the gas phase above the HTF was achieved through the venting. Internal estimations state that the concentration should be lowered to well below 100 ppm to enable back-permeation from the HCE to the HTF. To reach a concentration this low, daily venting is required. A time table applicable for the daily venting frequency, in which the expansion vessel cooldown takes place at night was set.

To detect a desired long-term reduction of HCE heat losses, the HCE temperatures are measured during operation. Two thermocouples were attached to the glass envelope of each HCE. The attachment of the thermocouples was affirmed by comparing the thermocouple measured temperatures with infrared drone measurements. With ALMEMO® dataloggers and the ALMEMO® Control 6.3 Software the temperatures are recorded minutely. The temperature data are merged and synchronized with the operating data of KONTAS. MatLab scripts were created to graphically visualize the HCE temperatures and KONTAS operation data. In the first week of operation the influence of wind and rain on the HCE temperatures was roughly examined. Based on the observed weather influences on the HCE temperatures a prefiltering of the data was developed to exclude values outside of the standard operation conditions. The graphical illustration of the prefiltered data could be used to visually detect long term changes of HCE temperatures. At the submission date of this thesis around 175 h of operation were reached. So far, no temperature reduction was notable.

The next steps of the experiment will be to continue the operation and perform daily venting with the suggested venting procedure. With weekly HTF sampling and remote analysis the hydrogen concentration in the HTF will be checked. If necessary the venting parameters or venting frequency should be adapted to maintain a hydrogen concentration well below 100 ppm in the HTF. As an effective hydrogen reduction would reduce the thermal losses of the receivers, the monitoring of the HCE temperatures during operation will provide a first indication of the condition of the HCEs. Once the 3000 h of operation are reached the experiment will be completed with a laboratory measurement of the HCEs heat losses at CIEMATs HEATREC test bench. With these measurements the performance restoration of the PTC receivers with hydrogen accumulation by back-permeation of hydrogen into HELISOL® XLP can be evaluated.

A limitation of the experiment is that the path of hydrogen in case of hydrogen reduction in the HCEs is not certainly known. Aside of back-permeation into the HTF also other permeation processes for example through the bellows of the HCEs to the atmosphere could occur. So, an evaluation of the back-permeation effectiveness might be imprecise. Also, a 24/7 operation at 400 °C is not realistic for operating power plants, so the required time to possibly improve the HCEs performance in power plants might differ significantly from the experiment at KONTAS. In solar thermal operation the concentration of solar light would lead to higher receiver tube temperatures, especially at the downside of the absorber tubes than in electrical operation of KONTAS. A higher receiver tube temperature could have a positive influence on the hydrogen permeation rate, but a negative influence on the getters hydrogen absorption capacity. Therefore, the electric operation of KONTAS during nighttime and malfunctioning of the tracking mechanism might impede the transferability of the experimental results to solar thermal operated power plants.

If an improvement of receiver performance by hydrogen reduction is demonstrated at KONTAS, further investigation in large-scale systems with similar operating conditions as in power plants should be conducted. A successful hydrogen reduction in a power plant would decrease the HCEs thermal losses which would improve the power plants thermal efficiency and might increase its income. In this case the performance restoration of receivers with hydrogen accumulation should be considered in technoeconomic assessments of an HTF changeover to silicone based HTF in operating power plants.

Nomenclature

Abbreviation list

BP.....*Biphenyl*
CIEMAT ..... Centro de Investigaciones Energéticas, Medioambientales y Tecnológicas
CSP..... *Concentrating Solar Power*
DLR..... *Deutsches Zentrum für Luft und Raumfahrt*
DNI.....*Direct Normal Irradiation*
DPO..... *Diphenyl Oxide*
GHG .....*Green House Gas*
GHS..... *Globally Harmonized System of Classification and Labeling of Chemicals*
HCE ..... Heat Collecting Element
HCU.....Heating and Cooling Unit
HTF.....*Heat Transfer Fluid*
IR..... *Infrared*
KONTAS .....*KOnzentrator Teststand Almeria Spanien*
LCOE .....*Levelized Cost of Energy*
LFR .....*Linear Fresnel reflectors*
MS.....*Molten Salt*
PB.....*Power Block*
PD ..... *Parabolic Dish*
PSA.....*Plataforma Solar de Almería*
PTC.....*Parabolic Trough Collector*
PV..... *Photovoltaic*
ST. ..... *Solar Tower*
TES .....Thermal Energy Storage
UN..... *United Nations*

List of figures

Figure 1: Types of CSP power plants. Credit: (International Energy Agency, 2010) 3
Figure 2: Schematic structure of a PTC power plant. Graphic from (Alami, Olabi et al. 2023)..... 4
Figure 3: PTC plant Andasol 2 with marked supply line (blue) and return line (red). Photo from Google maps, based on (Mehos et al., 2020) 5
Figure 4: Working Principle of PTC. Credit for photo: DLR (edited) 6
Figure 5: Cross-section of Heat Collecting Element 7
Figure 6: structure of Heat Collecting Element (photo on the left from SCHOTT Solar CSP GmbH) 7
Figure 7: Hydrogen formation of HELISOL® 5A and DPO/BP (Wacker Chemie AG, 2020)..... 10
Figure 8: Hydrogen generation and permeation in HCEs. Graphic from (Li et al., 2012)..... 11
Figure 9: Conduction heat loss and Knudsen number as a function of the annulus pressure for an HTF temperature of 350 °C (Lei, Ren, & Wang, 2020)..... 12
Figure 10: total heat loss and glass envelope temperature as a function of the hydrogen annulus pressure (Lei, Ren, & Wang, 2020)..... 13
Figure 11: Receiver heat losses of unused and an in-service receiver at different temperatures (Glatzmaier, Cable, & Newmarker, 2017) 14
Figure 12: Hydrogen removal from HTF by flushing expansion vessel with nitrogen. Source: modified, following (Glatzmaier, 2010))..... 15
Figure 13: Receivers heat loss reduction after heating (Glatzmaier, Cable, & Newmarker, 2017) 17
Figure 14: Heat loss of used and heated receiver in comparison to new receiver (Glatzmaier, 2020) 17
Figure 15: KONTAS facility at the Plataforma Solar de Almería, Spain (owned and operated by CIEMAT)..... 18
Figure 16: structure of KONTAS 19
Figure 17: Schematic structure of HTF sampling station (1), HTF recirculation (2) and gas venting lines (3) at KONTAS..... 20
Figure 18: Installed HTF sampling station (green), HTF recirculation (orange) and gas venting lines (yellow) installed at KONTAS (prior to installation of insulation) 21
Figure 19: Attachment of thermocouples to glass envelope of HCE 22
Figure 20: Schematic structure of HCE temperature measurement system at KONTAS..... 23
Figure 21: Ratio of condensation mass per vented nitrogen mass..... 26
Figure 22: Close up of the HTF sampling station (prior to the installation of thermal insulation) 28
Figure 23: Graph of HCE temperatures, ambient conditions and KONTAS parameter 31
Figure 24: Effect of weather conditions on HCE temperatures 31
Figure 25: Graph of prefiltered data for visual analysis of HCE temperature changes..... 32
Figure 26: Infrared image of the HCE temperatures at KONTAS during operation 33

List of tables

Table 1: KONTAS general characteristics and design operation range 19
Table 2: Operation parameter of KONTAS 24
Table 3: Results of condensate measurement for venting temperatures of 50 °C to 200 °C 25
Table 4: Concentrations in the HTF samples' gas phase before and after venting 29
Table 5: Time schedule for daily venting procedure 30
Table 6: Comparison of thermocouple and IR measured HCE temperatures 34

List of references

Acatech/Leopoldina/Akademienunion. (2022). *Accelerating the Expansion of Wind and Solar Power*. Science-based Policy Advice https://en.acatech.de/publication/expansion-wind-solar-power/

Alami, A. H., Olabi, A. G., Mdallal, A., Rezk, A., Radwan, A., Rahman, S. M. A., Shah, S. K., & Abdelkareem, M. A. (2023). Concentrating solar power (CSP) technologies: Status and analysis. *International Journal of Thermofluids*, *18*. https://doi.org/10.1016/j.ijft.2023.100340

Awan, A., Khan, M. N., Zubair, M., & Bellos, E. (2020). Commercial parabolic trough CSP plants: Research trends and technological advancements. *Solar Energy*, *211*, 1422-1458. https://doi.org/10.1016/j.solener.2020.09.072

Beckers, K. F., & Glatzmaier, G. C. (2018a). Addressing solar power plant heat transfer fluid degradation: Experimental measurements of hydrogen transport properties in binary eutectic biphenyl/diphenyl ether. *Solar Energy*, *173*, 304-312. https://doi.org/10.1016/j.solener.2018.07.066

Beckers, K. F., & Glatzmaier, G. C. (2018b). Modeling and simulating diffused aeration for hydrogen removal from expansion tanks of parabolic trough solar thermal power plants. https://doi.org/https://doi.org/10.1063/1.5067017

Burkholder, & Kutscher. (2009). *Heat Loss Testing of Schott's 2008 PTR70 Parabolic Trough Receiver*. https://www.nrel.gov/docs/fy09osti/45633.pdf

C. Hilgert (DLR), C. J. D., L. Valenzuela (CIEMAT), E. Schaffer (WACKER), D. Lei (IEECAS). (2021). *Silicone-Based Heat Transfer Fluids (SiHTF) in Line Focusing Concentrating Solar Power Applications* https://www.solarpaces.org/wp-content/uploads/Guideline_SiHTF_V1.0.pdf

Dersch, J., Dieckmann, S., Hennecke, K., Pitz-Paal, R., Taylor, M., & Ralon, P. (2020). LCOE reduction potential of parabolic trough and solar tower technology in G20 countries until 2030. *SOLARPACES 2019: International Conference on Concentrating Solar Power and Chemical Energy Systems*. https://doi.org/https://doi.org/10.1063/5.0028883

Desai, N. B., & Bandyopadhyay, S. (2016). Line-focusing concentrating solar collector-based power plants: a review. *Clean Technologies and Environmental Policy*, *19*(1), 9-35. https://doi.org/10.1007/s10098-016-1238-4

DJI. (2018). https://www.dji.com/de/zenmuse-xt2/specs

Espinosa-Rueda, G., Navarro Hermoso, J. L., Martínez-Sanz, N., & Gallas-Torreira, M. (2016). Vacuum evaluation of parabolic trough receiver tubes in a 50 MW concentrated solar power plant. *Solar Energy*, *139*, 36-46. https://doi.org/10.1016/j.solener.2016.09.017

Forristall, R. (2003). *Heat Transfer Analysis and Modeling of a Parabolic Trough Solar Receiver Implemented in Engineering Equation Solver*. https://www.nrel.gov/docs/fy04osti/34169.pdf

Giaconia, A., Tizzoni, A. C., Sau, S., Corsaro, N., Mansi, E., Spadoni, A., & Delise, T. (2021). Assessment and Perspectives of Heat Transfer Fluids for CSP Applications. *Energies*, *14*(22). https://doi.org/https://doi.org/10.3390/en14227486

Glatzmaier, G. (2020). *Acciona Power Plant Hydrogen Mitigation Project*. https://www.nrel.gov/docs/fy20osti/73168.pdf.

Glatzmaier, G. C. (2010). *Measurement of Hydrogen Purge Rates in Parabolic Trough Receiver Tubes* SolarPACES 2010, Perpignan, France. https://www.nrel.gov/docs/fy11osti/49366.pdf

Glatzmaier, G. C. (2013). *Systems and methods for selective hydrogen transport and measurement* (United states Patent No. https://www.osti.gov/servlets/purl/1107787

Glatzmaier, G. C. (2018). Hydrogen sensor for parabolic trough expansion tanks. https://doi.org/https://doi.org/10.1063/1.5067022

Glatzmaier, G. C., & Beckers, K. F. (2022). Hydrogen mitigation process testing at Nevada solar one. *International Conference on Advances in Multi-Disciplinary Sciences and Engineering Research: Icamser-2021*. https://doi.org/https://doi.org/10.1063/5.0086416

Glatzmaier, G. C., Cable, R., & Newmarker, M. (2017). Long-term heating to improve receiver performance. https://doi.org/https://doi.org/10.1063/1.4984330

International Energy Agency. (2010). *Technology Roadmap - Concentrating Solar Power*. https://www.iea.org/reports/technology-roadmap-concentrating-solar-power

International Energy Agency. (2023). *CO2 Emissions in 2022*. https://www.iea.org/reports/co2-emissions-in-2022

IPCC. (2022). Mitigation of Climate Change, Summary for Policymakers. https://doi.org/https://doi.org/10.1017/9781009157926.001

IRENA. (2022a). *Renewable Power Generation Costs in 2021*.

IRENA. (2022b). *World Energy Transitions Outlook 2022: 1.5°C Pathway*. https://www.irena.org/Energy-Transition/Outlook

John A. Duffie, W. A. B. (2013). Applications. In *Solar Engineering of Thermal Processes* (pp. 477-477). https://doi.org/https://doi.org/10.1002/9781118671603.part2

Jung, C., Dersch, J., Nietsch, A., & Senholdt, M. (2015). Technological Perspectives of Silicone Heat Transfer Fluids for Concentrated Solar Power. *Energy Procedia*, *69*, 663-671. https://doi.org/10.1016/j.egypro.2015.03.076

Jung, C., Hilgert, C., Schickedanz, K., Schaffer, E., Weidner, R., Moxter, M., Saur, M., Ortiz Vives, F., Wasserfuhr, C., & Schmitz, M. (2018). Abschlussbericht zum verbundvorhaben SITEF - Silicone Fluid Test facility. https://doi.org/https://doi.org/10.2314/GBV:1663361460

Jung, C., & Senholdt, M. (2020). Comparative study on hydrogen issues of biphenyl/diphenyl oxide and polydimethylsiloxane heat transfer fluids. *SOLARPACES 2019: International Conference on Concentrating Solar Power and Chemical Energy Systems*. https://doi.org/https://doi.org/10.1063/5.0028894

Jung, C., Senholdt, M., Spenke, C., Schmidt, T., & Ulmer, S. (2019). Hydrogen monitoring in the heat transfer fluid of parabolic trough plants. *SOLARPACES 2018: International Conference on Concentrating Solar Power and Chemical Energy Systems*. https://doi.org/https://doi.org/10.1063/1.5117599

Jung, C., & Spenke, C. (2022). Hydrogen monitoring and control in the heat transfer fluid of parabolic trough plants. *SOLARPACES 2020: 26th International Conference on Concentrating Solar Power and Chemical Energy Systems*. https://doi.org/https://doi.org/10.1063/5.0085825

Krishna, Y., Faizal, M., Saidur, R., Ng, K. C., & Aslfattahi, N. (2020). State-of-the-art heat transfer fluids for parabolic trough collector. *International Journal of Heat and Mass Transfer*, *152*. https://doi.org/10.1016/j.ijheatmasstransfer.2020.119541

Krüger, D., Detzler, R., Schmitz, M., Jung, C., Bonk, A., Hanke, A., Horta, P., Martins, P., Torabzagedan, M., & Stengler, J. (2024). Operating Parabolic Troughs With Molten Salt: Solar Field Optimisation and Ternary Salt Properties. *SolarPACES Conference Proceedings*, *1*. https://doi.org/10.52825/solarpaces.v1i.689

Kuckelkorn, T., Jung, C., Gnädig, T., Lang, C., & Schall, C. (2016). Hydrogen generation in CSP plants and maintenance of DPO/BP heat transfer fluids – A simulation approach. https://doi.org/https://doi.org/10.1063/1.4949187

Lang, C., Belkheir, M., Kim, E., Davidson, C., Holden, B., & Hook, B. (2017). Hydrogen reduction in heat transfer fluid in parabolic trough CSP plants. https://doi.org/https://doi.org/10.1063/1.4984501

Lei, D., Ren, Y., & Wang, Z. (2020). Numerical study of conduction and radiation heat losses from vacuum annulus in parabolic trough receivers. *Frontiers in Energy*, *16*(6), 1048-1059. https://doi.org/10.1007/s11708-020-0670-7

Li, J., Wang, Z., Lei, D., & Li, J. (2012). Hydrogen permeation model of parabolic trough receiver tube. *Solar Energy*, *86*(5), 1187-1196. https://doi.org/10.1016/j.solener.2012.01.011

Lilliestam, J., Ollier, L., Labordena, M., Pfenninger, S., & Thonig, R. (2020). The near- to mid-term outlook for concentrating solar power: mostly cloudy, chance of sun. *Energy Sources, Part B: Economics, Planning, and Policy*, *16*(1), 23-41. https://doi.org/10.1080/15567249.2020.1773580

Márquez, J. M., López-Martín, R., Valenzuela, L., & Zarza, E. (2016). Test bench HEATREC for heat loss measurement on solar receiver tubes. https://doi.org/https://doi.org/10.1063/1.4949077

Mehos, M., Price, H., Cable, R., Kearney, D., Kelly, B., Kolb, G., & Morse, F. (2020). *Concentrating Solar Power Best Practices Study*. https://www.nrel.gov/docs/fy20osti/75763.pdf

Moens, L., & Blake, D. (2010). Mechanism of Hydrogen Formation in Solar Parabolic Trough Receivers. *Journal of Solar Energy Engineering-transactions of The Asme - J SOL ENERGY ENG*, *132*. https://doi.org/10.1115/1.4001402

Moosavian, S. F., Hajinezhad, A., Fattahi, R., & Shahee, A. (2023). Evaluating the effect of using nanofluids on the parabolic trough collector's performance. *Energy Science & Engineering*. https://doi.org/10.1002/ese3.1537

Naresh, G., Rajasekhar, A., Bharali, J., & Ramesh, K. (2022). Homogeneous molten salt formulations as thermal energy storage media and heat transfer fluid. *Journal of Energy Storage*, *50*. https://doi.org/10.1016/j.est.2022.104200

National Renewable Energy Laboratory. (2022). https://solarpaces.nrel.gov/by-technology

Navas, S. J., Ollero, P., & Rubio, F. R. (2017). Optimum operating temperature of parabolic trough solar fields. *Solar Energy*, *158*, 295-302. https://doi.org/https://doi.org/10.1016/j.solener.2017.09.022

NREL. (2024). *Concentrating Solar Power Projects*. https://solarpaces.nrel.gov/by-project-name

Orvalho, H. M. d. S. R. (2009). *Hydrogen Permeation in Parabolic Trough Receivers* Universidade Nova de lisboa]. http://hdl.handle.net/10362/13739

Pan, C. A., Ferruzza, D., Guédez, R., Dinter, F., Laumert, B., & Haglind, F. (2018). Identification of optimum molten salts for use as heat transfer fluids in parabolic trough CSP plants. A techno-economic comparative optimization. https://doi.org/https://doi.org/10.1063/1.5067028

REN21. (2023). Renewables in Energy Supply. *Renewables 2023 Global Status Report collection ISBN 978-3-948393-08-3*.

Resch, G., Schöniger, F., Kleinschmitt, C., Franke, K., Thonig, R., & Lilliestam, J. (2022). Deep decarbonization of the European power sector calls for dispatchable CSP. *SOLARPACES 2020: 26th International Conference on Concentrating Solar Power and Chemical Energy Systems*. https://doi.org/https://doi.org/10.1063/5.0086710

Schaffer, Dersch, Dörrich, Hilgert, & Jung. (2016). *HELISOL® - ein Siliconöl basierter Wärmeträger für CSP Kraftwerke* https://www.dlr.de/sf/Portaldata/73/Resources/dokumente/soko/soko2016/DLR-Sonnenkolloquium2016_Schaffer_(Wacker)_HELISOL-Ein_Siliconoel_fuer_CSP_Kraftwerke.pdf

Schaffer, E. (2020). *Condition Monitoring for the Use of Silicone Oil as a Heat Transfer Medium* DLR Sonnenkolloquium, https://www.dlr.de/de/sf/downloads/dokumente/soko/soko2020/Silicone_Oil_Schaffer.pdf/@@download/file

Schöniger, F., Thonig, R., Resch, G., & Lilliestam, J. (2021). Making the sun shine at night: comparing the cost of dispatchable concentrating solar power and photovoltaics with storage. *Energy Sources, Part B: Economics, Planning, and Policy*, *16*(1), 55-74. https://doi.org/10.1080/15567249.2020.1843565

Tagle-Salazar, P. D., Nigam, K. D. P., & Rivera-Solorio, C. I. (2020). Parabolic trough solar collectors: A general overview of technology, industrial applications, energy market, modeling, and standards. *Green Processing and Synthesis*, *9*(1), 595-649. https://doi.org/10.1515/gps-2020-0059

TC Mess- und Regeltechnik GmbH. (2024). https://www.tcgmbh.de/thermoelemente/typ-k-thermoelemente.html

UNFCCC. (2023). *COP28 Agreement Signals "Beginning of the End" of the Fossil Fuel Era*. https://unfccc.int/news/cop28-agreement-signals-beginning-of-the-end-of-the-fossil-fuel-era

Wacker Chemie AG. (2020). HELISOL XLP extended technical datasheet. https://www.wacker.com/h/en-us/medias/2_HELISOL_XLP_extended_technical_data.pdf

Wacker Chemie AG. (2020). HELISOL Technical Product Brochure. https://www.wacker.com/h/de-de/medias/4_HELISOL_Technical_Product_Brochure.pdf

Wehner, K. (2022). *Techno-economic evaluation of a full heat transfer fluid change-over in an existing parabolic trough power plant* Technische Universität Darmstadt]. https://elib.dlr.de/189102/

Yao, F., Lei, D., Yu, K., Han, Y., Yao, P., Wang, Z., Fang, Q., & Hu, Q. (2019). Experimental Study on Vacuum Performance of Parabolic Trough Receivers based on a Novel Non-destructive Testing Method. *Energies*, *12*(23). https://doi.org/10.3390/en12234531

Yokogawa Electric Corporation. (2022). *Hydrogen Permeation*. https://www.yokogawa.com/us/library/resources/application-notes/hydrogen-permeation/